

Recent Progress in the Consistent Interpretation of Complementary Spectroscopic Results Obtained on Molecular Systems

Roman Forker, Marco Gruenewald, Tino Kirchhübel, and Torsten Fritz*

Dedicated to Professor Karl Leo on the occasion of his 60th birthday

Research on organic thin films is largely driven by potential (opto-)electronic applications and turns out to be no less intriguing from a fundamental point of view. Numerous studies make it clear that the understanding of device-relevant molecular thin film architectures is quite challenging—often hampered by insufficient spectroscopic data and the lack of a consistent interpretation of the available datasets. Consequently, speculative aspects prevail in the discussion of energy levels in conjunction with the optical properties of organic thin films. Adequate spectroscopic techniques applicable to thin films of organic molecules (typical thicknesses required for devices are in the nanometer range) with the necessary sensitivities are rather demanding. Some of those methods were developed or significantly improved in the recent past. Here, the now available complementary spectroscopies are briefly surveyed with particular emphasis on some techniques that have not yet become widespread standards, and a non-exhaustive set of examples of acquired experimental results are provided. For a consistent interpretation of the latter, the concepts brought forward in the literature considering the role of initial and final states of spectroscopic processes are outlined, with important consequences for quantitatively correct energy diagrams.

diodes)^[1] are now commercially available, while others (such as organic photovoltaic devices)^[2] are about to attain a broader perception. Although the progress already achieved for such devices is promising and certainly motivating, the detailed understanding of the physical processes determining their efficiencies (and thus, further improvement) is still challenging. This has several causes, some of which are listed in the following.

First, high-purity reference samples are much more difficult to obtain because of the often limited possibilities of thermal or chemical purification of many organic compounds in comparison to inorganic semiconductor materials. Unintended impurities tend to act as traps,^[3,4] and they sometimes obscure spectroscopic measurements of the host material (see also below).


Second, to get a full and consistent picture of the structure–property relations is much more complicated than for inorganic semiconductors, mainly due to:

1. Introduction

Organic optoelectronic devices are intensively studied by international research communities. Some developments have matured, and many products (such as organic light-emitting

- the strong tendency of many organic materials to exhibit polymorphism,^[5–7]
- the more complicated transport mechanisms, ranging from hopping for poorly and moderately ordered samples to band transport for pristine organic crystals,^[8]
- the much higher doping concentrations required for appropriate electrical conductivities^[9–12] (in particular, difficulties arise from the fact that doping is likely to cause structural alterations in the non-covalently bound organic solids),^[13–15]
- the many-body problem to be solved for typical organic molecules containing dozens of atoms (hence requiring many approximations) in case theoretical input is sought, and conversely, the inappropriateness of the single-particle picture,^[16,17]
- the high exciton binding energies involved,^[18,19] which makes it much more difficult to separate charge carriers in photovoltaics, for example.^[2] In addition, we note that the exciton binding energies vary considerably among different organic semiconducting materials,^[18,19] which requires an even more sophisticated treatment.

Dr. R. Forker, Dr. M. Gruenewald, T. Kirchhübel, Prof. T. Fritz
Friedrich Schiller University Jena
Institute of Solid State Physics
Helmholtzweg 5, Jena 07743, Germany
E-mail: torsten.fritz@uni-jena.de

 The ORCID identification number(s) for the author(s) of this article can be found under <https://doi.org/10.1002/adom.202100200>.

© 2021 The Authors. Advanced Optical Materials published by Wiley-VCH GmbH. This is an open access article under the terms of the Creative Commons Attribution-NonCommercial License, which permits use, distribution and reproduction in any medium, provided the original work is properly cited and is not used for commercial purposes.

DOI: 10.1002/adom.202100200

Third, adequate spectroscopic techniques applicable to thin films of organic molecules (typical thicknesses required for devices are in the nanometer range) with the necessary sensitivities are rather demanding:

- Some of those techniques were developed or significantly improved only recently and have not yet become widespread standards even in research laboratories specializing in surface science. Hence, some of those less frequently used methods are not yet commercially available as a ready-to-use apparatus.
- Often, different available photoelectron spectroscopies are applied by different research groups on similar samples, for example, to determine the highest occupied and lowest unoccupied molecular orbitals (HOMO and LUMO, respectively). As we will discuss in detail, the comparison of the data obtained is often confusing and prone to discrepancies if the influence of the particular measurement method, expressed by the specific initial and final states involved, is not accounted for.
- Especially for organic solids, it is difficult if not impossible to extract the optical properties of a sample directly from its electronic structure or vice versa, one reason being again the rather large exciton binding energy.^[20] In many cases, researchers are aware of the drawbacks resulting from insufficient spectroscopic data.^[21–23] Therefore, complementary techniques are required for a full characterization.

The understanding of device-relevant organic thin film architectures is hampered by fragmentary spectroscopic data and the lack of a consistent interpretation of the available datasets, which often leaves no choice but to make rather uncertain assumptions. Consequently, some speculative aspects prevail in the discussion of energy levels in conjunction with the optical properties of organic thin films, where clearer interpretations would be possible if one employs the now available set of complementary spectroscopic techniques and applies the concepts recently brought forward in the literature considering the role of initial and final states of spectroscopic processes in order to obtain quantitatively accurate energy level diagrams.^[16,17,24]

To assist and to guide the reader, we precede this analysis with a brief survey of some of the most important surface-sensitive spectroscopic techniques to date. We deem this important, since recent methodological developments provided the means for filling some experimental gaps, namely the demand for reliable data for the unoccupied levels as well as for the optical transition energies of very thin organic films.

2. Complementary Spectroscopic Techniques

We begin our assessment with an overview of selected optical and electron spectroscopies frequently used to characterize thin molecular films (**Figure 1**). The techniques compiled in this scheme are: ultraviolet photoelectron spectroscopy (UPS), two-photon photoelectron spectroscopy (2PPE), inverse photoelectron spectroscopy (IPES), and optical absorption spectroscopy. Note that photoelectron spectroscopy (PES) or one-photon photoelectron spectroscopy is sometimes used synonymously

for UPS, albeit not restricted to a specific spectral range. Other techniques, such as electrochemical measurements,^[25,26] are beyond the scope of this perspective.

In the following, we summarize the above spectroscopies and discuss previously published data mainly for pentacene (CAS registry number: 135-48-8) and for the stacked heteromolecular system copper(II)-phthalocyanine (CuPc, CAS registry number: 147-14-8) on 3,4,9,10-perylenetetracarboxylic dianhydride (PTCDA, CAS registry number: 128-69-8) on Ag(111).

2.1. Photoelectron/Photoemission Spectroscopy

In the toolbox of surface-sensitive spectroscopic techniques UPS is among the most cultivated and widely used. Given the abundance of literature on this subject, we refer the reader to several review articles.^[27–31] Typical instrumentations, experimental resolutions, as well as theoretical treatments are detailed in the above articles and references therein.

For the scope of this perspective, it is important to discuss some peculiarities of the experimental UPS data acquired for organic molecules and thin films thereof. As a specific example, **Figure 2** displays the UP spectra of pentacene associated with the HOMO (more precisely: the probe process H_0^+ , compare **Figure 1**). These results were compiled previously^[30] from measurements of dissimilar types of samples, namely pentacene in the gas phase, face-on monolayers (ML) on highly oriented pyrolytic graphite (HOPG), standing disordered films on SiO_2 , and standing crystalline films on CuPc on HOPG.^[30,32–34] Those spectra are shifted on the abscissa to facilitate a direct comparison.^[30] The center of the main peak of the gas-phase data (**Figure 2a**) defines the value 0 eV on the relative energy scale. In the same way, the main peaks of the ML data (**Figure 2b,c**) are aligned with 0 eV. Finally, the much broader spectra of the standing films (**Figure 2d,e**) are aligned such that their energetically upper and lower half maximum values are equidistant with respect to 0 eV.

Some characteristics of these data are especially noteworthy: One can easily see that the gas-phase spectra exhibit the narrowest peaks, although those molecules are at much higher temperatures than in all other measurements, especially when compared to the low-temperature spectrum ($T = 49$ K) on HOPG. Given that all spectra in **Figure 2** (except for the red solid line) were recorded in the group of Ueno and Kera using the same electron energy analyzer and the same HeI light source, one can infer similar instrumental broadening in those data.^[30] Therefore, thermal broadening is not the dominant cause of the observed spectral widths, particularly of the curves in **Figure 2d,e**. Instead, the width of the curve for the crystalline film (**Figure 2e**) is dominated by the dispersion of the HOMO-derived electronic band and the fact that angle-integrated data are displayed.^[30] The band formation is caused by the non-negligible transfer integrals between neighboring molecules in the standing adsorption motif of pentacene on CuPc/HOPG as suggested in **Figure 2**. The disordered film (**Figure 2d**) exhibits additional inhomogeneous broadening. Furthermore, we emphasize that the absolute energies of the spectra in **Figure 2** are different, as expressed by the ionization energies (IE) indicated for each spectrum.

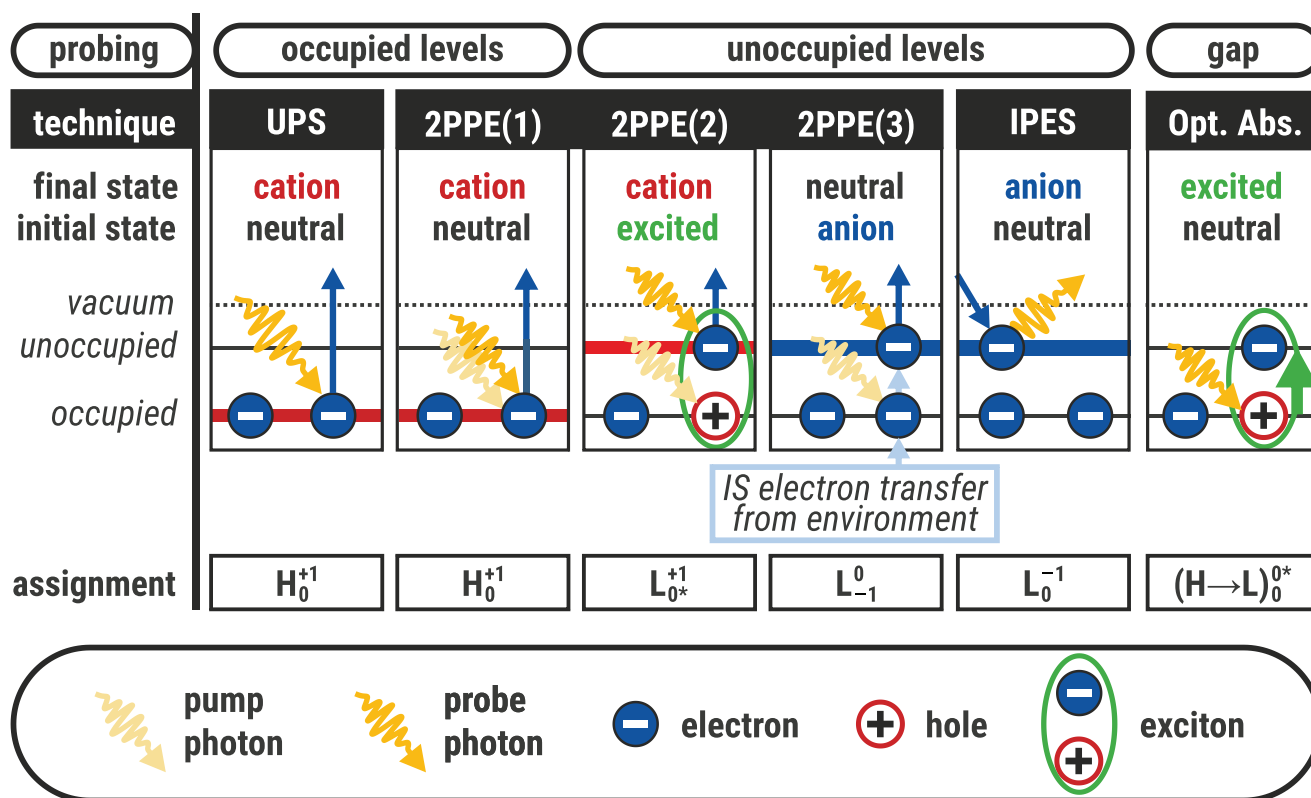


Figure 1. Schematic overview of important optical and electron spectroscopies used to characterize thin molecular films. For the sake of simplicity, only the highest occupied and the lowest unoccupied molecular orbitals (abbreviated H and L, respectively) are depicted. The first of two photons in 2PPE puts the molecule in an “intermediate state” (IS), which is then probed by the second photon. Note that the process 2PPE(3) involves a photohole quenching in the intermediate state of the molecule due to electron transfer from its environment (e.g., from the substrate). For all probe processes the initial and final states are given, where the assignments employ the labeling scheme $LEVEL_{\text{initial state}}^{\text{final state}}$ suggested previously.^[17] Adapted with permission.^[17] Copyright 2019, Royal Society of Chemistry.

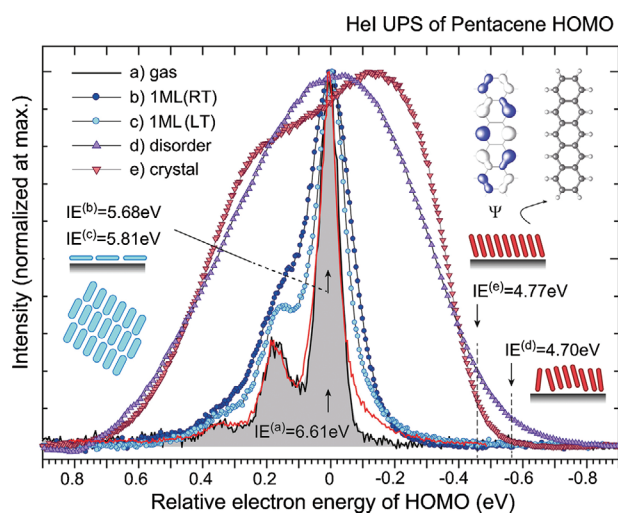


Figure 2. Compilation of UPS data associated with the HOMO (H_0^{+1}) of pentacene; see the upper right inset for the molecular structure. a) Spectra acquired for gas-phase molecules: black curve at 433 K,^[30] red curve at 508 K.^[32] b) Face-on monolayer on HOPG at 295 K and c) at 49 K.^[33] d) Standing disordered film, $d = 1$ nm on SiO_2 , and e) standing crystalline film, $d = 1.5$ nm on CuPc/HOPG , both at 295 K.^[34] All spectra are aligned with the main peak of the gas-phase data and displayed on a relative energy scale. Note that the absolute energies are different, as expressed by the ionization energies (IE) indicated for each spectrum. Reproduced with permission.^[30] Copyright 2015, Elsevier.

For a crystalline thin film phase of lying-down pentacene (film thickness $d = 12$ nm) directly on HOPG, the HOMO-derived band dispersion was measured by Koch et al. using angle- and energy-resolved UPS (Figure 3).^[35] The band structure $E(\vec{k})$ of molecular aggregates can often be described in the framework of a tight-binding model, where the strength of the orbital overlap between neighboring molecules (as expressed by the transfer integral t) is related to the bandwidth $W = E_{\text{max}} - E_{\text{min}}$. Due to the anisotropy frequently encountered in organic thin film structures, said orbital overlap and thus the band structure can differ markedly in the directions parallel (x, y) and perpendicular (\perp) to the substrate surface, for example. Measuring the photoelectron intensity as a function of the polar and azimuthal emission angles (along with the kinetic energy) yields the band structure $E(k_x, k_y)$ parallel to the substrate surface.^[27,28] Correspondingly, the variation of the incoming photon energy $h\nu$ can be employed to assess the band structure $E(k_\perp)$ perpendicular to the substrate surface.^[35]

On closer inspection, the angle-integrated UPS data of an essentially face-on oriented ML of pentacene on HOPG (Figure 2b,c) are only slightly broader than the gas-phase spectra (Figure 2a) and still exhibit the vibronic substructure. This is consistent with rather weak orbital overlap between lateral pentacene neighbors (and also weak adsorbate–substrate interactions) and hence an essentially absent dispersion. By contrast, the nominal pentacene film thickness in Figure 3 is

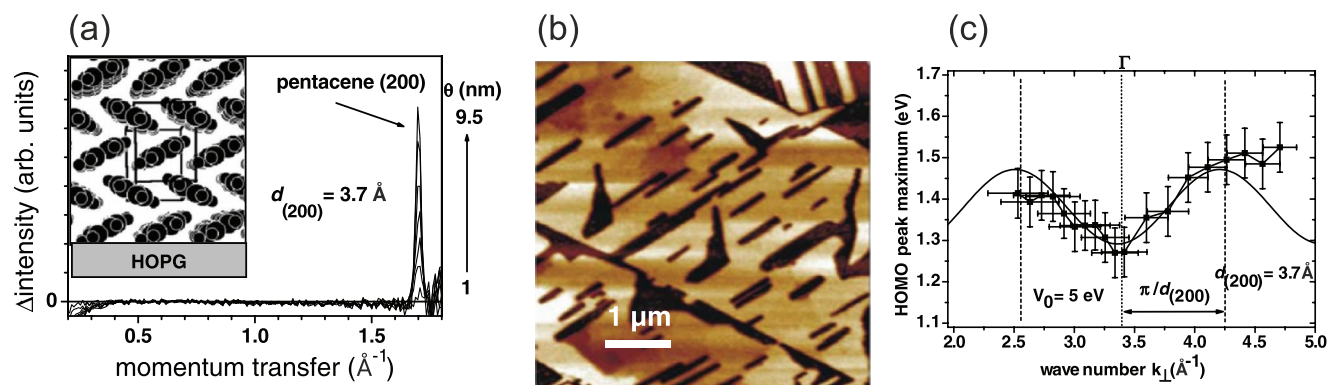


Figure 3. a) X-ray diffraction data of pentacene on HOPG for various film thicknesses θ . The inset depicts the molecular orientation and the pentacene unit cell. b) Atomic force microscopy image of a nominally 12 nm thick pentacene film on HOPG. c) Dispersion of the HOMO-derived band of pentacene on HOPG at 120 K acquired via angle- and energy-resolved UPS. The cosine curve $E_B(k_{\perp}) = E_{B,0} - 2t \cos(a_1 k_{\perp})$ represents a fit using a tight-binding model. The bandwidth amounts to $W = 4t$, where $t \approx 50$ meV is the transfer integral. The dispersion at 297 K is similar (not shown here). Reproduced with permission.^[35] Copyright 2006, American Physical Society.

12 nm, which means multiple stacked molecular layers in the lying-down orientation. Consequently, although the lateral intermolecular orbital overlap is still very weak, the overlap in the stacking direction (i.e., perpendicular to the substrate surface) is noticeably stronger, as evidenced by the dispersion depicted in Figure 3c. This has immediate consequences for the discussion of energy levels. As opposed to a lying-down pentacene ML, the HOMO-derived feature of a comparatively thick lying-down pentacene sample is found at a binding energy that depends on k_{\perp} and hence on the measurement conditions. The bandwidth W of this HOMO-derived feature amounts to ≈ 0.2 eV and is therefore not negligible.

In the light of the above remarks, we reiterate the importance of the structure–property relations of organic solids, as expressed here by the differences in the absolute IE, the spectral appearances (e.g., vibronic substructure), and the possible formation of electronic bands. These circumstances call for structural and spectroscopic characterizations to complement one another.

2.2. Inverse Photoelectron/Photoemission Spectroscopy

IPES denotes the photon emission following the injection of an electron into an unoccupied level of the sample. IPES resurged just recently owing to some significant improvements of the necessary components.^[36–40] Especially the previously employed MeF₂ windows (Me = alkaline earth metal) serving as a bandpass in combination with alkali-halide-sensitized electron multipliers exhibit rather high center energies of ≈ 9 –10 eV.^[41,42] Therefore, comparatively high kinetic electron energies E_{kin} were required to perform this kind of spectroscopy, which are likely to cause radiation damage to the sensitive organic samples (see below). Using multilayer dielectric interference filters instead allows for photon bandpass center energies well below 5 eV, cf. Figure 4. From energy conservation it follows that $h\nu - E_{\text{kin}} = E_{\text{vac}} - \epsilon_{\text{unocc}}$, where E_{vac} denotes the vacuum level and ϵ_{unocc} the probed unoccupied level. Thus, higher optical bandpass energies $h\nu$ require higher kinetic energies E_{kin} . In order to demonstrate the effect of low and high E_{kin} , Yoshida

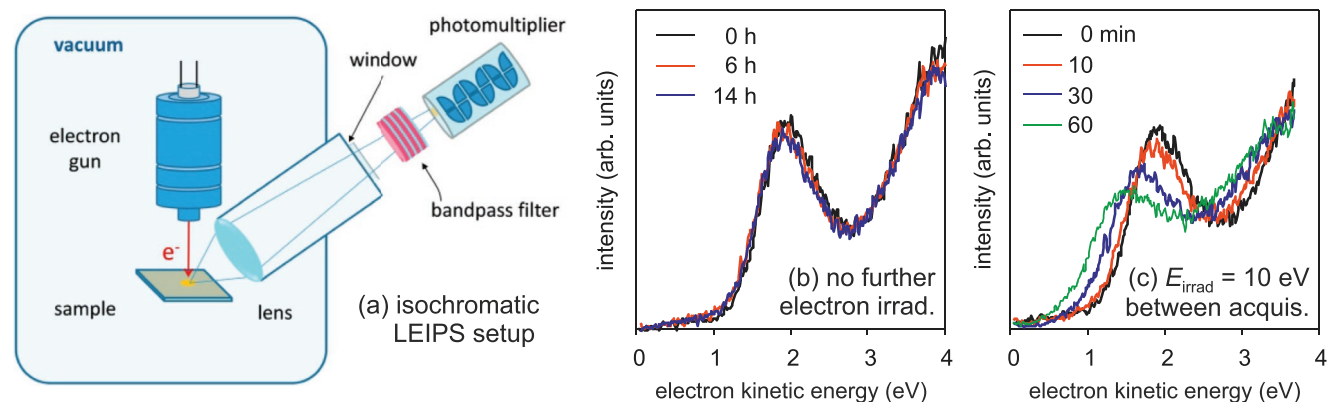


Figure 4. a) Scheme of an isochromatic LEIPS setup. The photon energy $h\nu$ is selected by a bandpass filter. Upon variation of the kinetic electron energy the spectra stemming from unoccupied levels of the sample are obtained. b,c) Spectra acquired for a thin CuPc film with the same LEIPS setup and with identical measurement conditions, that is, the kinetic energy of the electrons was varied between $E_{\text{meas}} = 0$ eV and ≈ 4 eV.^[36] These energies correspond to NUV photon detection. The sample in (b) was not exposed to additional electron irradiation. The sample in (c) was additionally irradiated with electrons (10 min, $E_{\text{irrad}} = 10$ eV, $j \approx 10^{-5}$ A cm⁻²) in between each data acquisition, which is meant to simulate the conditions of earlier IPES setups that detected VUV photons. Note the absence of spectral changes in (b) as opposed to (c). Adapted with permission.^[39] Copyright 2015, Elsevier.

compared two similar experiments for a thin CuPc film using the same setup and identical measurement conditions, that is, the kinetic energy of the electrons was varied between $E_{\text{meas}} = 0$ and ≈ 4 eV.^[36] In the first experimental run, no additional electron irradiation was applied, meaning that the sample was exposed to kinetic electron energies no greater than 5 eV, which is called the near-ultraviolet (NUV) photon detection mode. The recorded spectra remained unchanged over the course of many hours, cf. Figure 4b. In the second experimental run, the same sample system was additionally irradiated with electrons $E_{\text{irrad}} = 10$ eV in between each data acquisition, so as to simulate the conditions of conventional IPES setups in the vacuum-ultraviolet (VUV) photon detection mode. As evidenced in Figure 4c, those conditions led to a clear broadening of the features and to spectral shifts in a matter of several minutes to a few hours. By comparison, the significantly reduced electron energies below 5 eV effectively minimize radiation damage and sample charging problems. Hence, this improved method was dubbed low-energy inverse photoemission spectroscopy (LEIPS).^[36–40] This technique has since been applied to several molecular thin films.^[11,43–48]

As an example, Figure 5 shows LEIPS data for pentacene ($d = 10$ nm) on HOPG and on silicon covered with natural oxide (SiO_2).^[40] Since the cross sections of inverse photoemission are several orders of magnitude inferior to direct photoemission,^[49,50] LEIPS data are typically much noisier. Furthermore, the instrumental broadening of LEIPS setups has several significant contributions, especially the energy spread of the electron gun ($\Delta E \approx 0.25$ eV for a BaO cathode at $T = 1150$ K) and the width of the employed bandpass (typical spectral width between 0.1 and 0.3 eV).^[36] Consequently, the experimental resolution typically achieved is not sufficient to discern possible vibronic

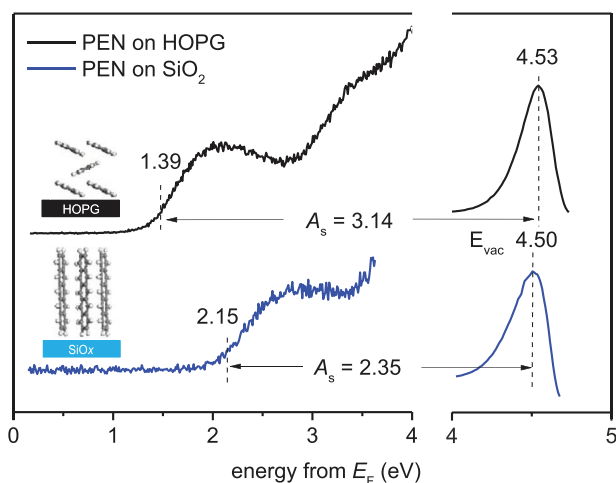


Figure 5. LEIPS data of pentacene ($d = 10$ nm) on HOPG and on naturally oxidized silicon. The photon energy was selected by a bandpass filter at a center energy of 4.38 eV. Insets depict the assumed molecular orientations consistent with atomic force microscopy images (not shown here). The peak closest to the Fermi energy is associated with the LUMO (L_0^-) of pentacene. Here, the electron affinities, A_s , were extracted from the peak onsets (dashed lines, see left-hand side). The position of the vacuum energy, E_{vac} , was determined from the first derivative of the simultaneously recorded sample current (see right-hand side). Reproduced with permission.^[40] Copyright 2015, American Physical Society.

substructures in LEIPS data. Nonetheless, the peak positions and onsets can readily be recognized in Figure 5. Although the vacuum level, E_{vac} , is almost identical for both samples, the electron affinity of pentacene on SiO_2 is significantly smaller than on HOPG, which was attributed by Yoshida et al. to different molecular orientations.^[40] A comparison of LEIPS to the aforementioned UPS data of pentacene^[30,35] reveals that both techniques unravel a dependence of the spectra on the molecular orientation and/or packing on the substrate.

2.3. Optical Spectroscopy

In differential reflectance spectroscopy (DRS) the relative change of the reflectance $R(E, d)$ of a sample covered with a film of thickness d is related to the reflectivity of the pristine substrate $R(E, d = 0)$, where E is the photon energy.^[51–53] The DRS signal is given as:

$$\text{DRS} \equiv \frac{\Delta R}{R}(E, d) := \frac{R(E, d) - R(E, d = 0)}{R(E, d = 0)} \quad (1)$$

The complex reflection coefficient \hat{r} and thus the reflectance $R = |\hat{r}|^2$ depend on the angle of incidence and the polarization of the light. However, in the case of normal or near-normal incidence of the light, as typically employed for DRS (cf. Figure 6), the polarization dependence is less important, and essentially the in-plane components of the dielectric tensor $\hat{\epsilon}$ are probed.

These in-plane components of $\hat{\epsilon}$ are especially relevant for the optimization of devices like organic solar cells, where flat-lying molecules (i.e., transition dipole moments parallel to the surface) are beneficial in terms of light harvesting.^[54,55] If the organic thin film exhibits differently rotated domains (e.g., mirror and rotational domains), these in-plane components behave quasi-isotropically. Randomly polarized light can thus be employed for DRS for the sake of simplicity. Compared with other methods, which exploit the polarization dependence of the sample reflectivity (e.g., reflection anisotropy

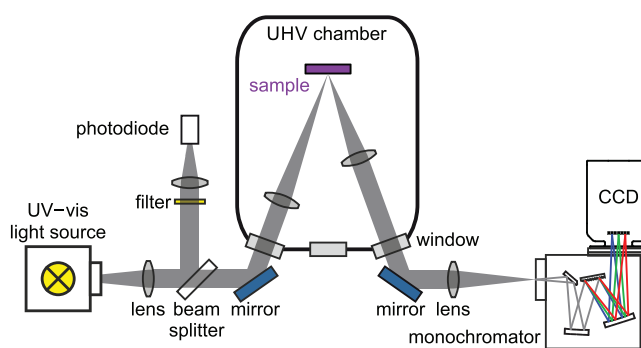


Figure 6. Scheme of a typical DRS setup (not to scale). UV-vis light is collimated at near normal incidence on a substrate surface, which itself is pointing downward. The reflected light is focused on the entrance slit of a monochromator. Reflectance spectra are recorded with a charge-coupled device (CCD). Such a measurement geometry allows for real-time acquisition of the gradual change in reflectance during the deposition of adsorbate layers. The photodiode simultaneously monitors the lamp intensity, whose fluctuations often cause signal drift.

spectroscopy^[56–58], the application of DRS is not restricted to samples with surface anisotropy. The difficulty in performing DRS arises from the requirement to measure the reflectivities with long-term stability, even though the absolute values are not required due to the normalization in Equation (1). Otherwise, one has to deal with baseline ($R(E, d = 0)$) drifts, which could easily be misinterpreted as absorption features in the DRS data. While such drifts potentially arise from various sources (mechanical, electric, and thermal influences), lamp intensity fluctuations seem to contribute primarily. This issue can be tackled by a two-beam setup (i.e., the lamp spectrum and the reflectance spectrum are measured simultaneously) such that DRS signals in the order of 10^{-4} can be detected reliably.^[59] It has been further demonstrated that DRS can be used most beneficially when performed in situ. For instance, the exposure of pentacene ML films to ambient conditions triggers degradation processes (e.g., recrystallization),^[60] which are often difficult to avoid when applying ex situ methods.

Further, in the case of flat-lying molecules the in-plane interaction of transition dipoles is much weaker than the coupling between consecutive layers, that is, in stacking direction. This gives rise to substantial spectral changes upon the beginning of the growth of the second ML in the sense that the first ML on a weakly interacting substrate usually reflects the spectral characteristics of single molecules while the spectra for higher coverages are dominated by out-of-plane excitonic interactions. Consequently, in situ DRS offers a convenient tool to control the thickness of the deposited organic layers.^[51,61]

As an example, Figure 7 shows DRS data for pentacene (PEN) on sapphire ($\alpha\text{-Al}_2\text{O}_3(0001)$).^[60] Up to a nominal thickness of 0.1 ML (here 1 ML refers to the full coverage of the substrate by a single layer of upright-standing pentacene molecules) faint features denoted as “c” and “d” were assigned to the HOMO–LUMO electronic transition of the molecule and vibronic replica. The more prominent features “e” and “f” are attributed to transitions from the HOMO to the LUMO+2 and to the LUMO+1, respectively. Since the corresponding transition dipole moments for “e” and “f” are both oriented along the long molecular axis,^[63] and the polarization plane of the incident light is parallel to the substrate surface, it was concluded that the molecules adsorb flat-lying on the surface. From 0.1 to 1.1 ML, significant excitonic coupling indicates the formation of a new phase comprising upright-standing molecules on top of the flat-lying wetting layer.^[60]

The presented DRS data compare favorably with other measurements (ex situ), for example, the DRS spectrum of the wetting layer is very similar to solvent data of the molecule (cf. inset in Figure 7, green dotted curve). This means that pentacene experiences weak interaction with the surrounding molecules as well as weak electronic interaction with the substrate. For the upright-standing molecules in the second layer, however, the spectra with the two Davydov components “a” and “b” resemble the in-plane optical absorption behavior of pentacene films, a few nanometers thick, on SiO_2 (cf. inset in Figure 7, blue solid curve) as measured by means of variable angle spectroscopic ellipsometry (VASE)^[64] and visible p-polarized multiple-angle incidence resolution spectrometry.^[65]

Comparisons with photoluminescence (PL) data are also insightful. The dominating PL line of pentacene, often referred

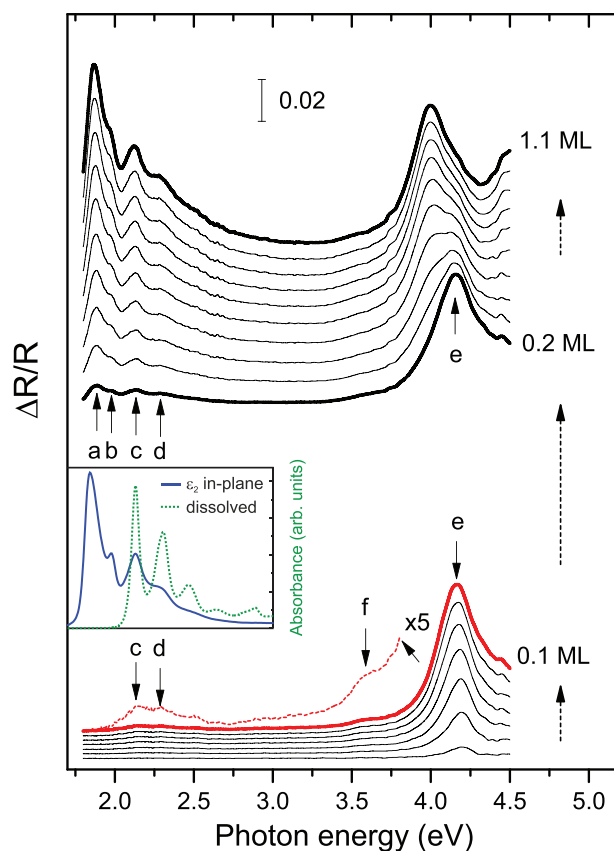


Figure 7. In situ DRS data of pentacene on sapphire ($\alpha\text{-Al}_2\text{O}_3(0001)$) acquired at 300 K. Initially, a dilute phase of flat-lying molecules is formed up to a nominal thickness of 0.1 ML (red thick line). Further molecules adopt an upright-standing orientation on top of the wetting layer up to completion of the second layer (total nominal thickness of 1.1 ML). Note that, in this case, 1 ML refers to the full coverage of the substrate by a single layer of upright-standing pentacene molecules. For clarity, subsequent spectra are vertically shifted by 0.001 and 0.01 in the lower and upper parts of the diagram, respectively. Adapted with permission.^[60] Copyright 2017, American Physical Society. The inset shows ex situ optical spectroscopy results for pentacene samples. Blue solid curve: in-plane component of the imaginary part, ϵ_2 , of the dielectric function of pentacene grown on SiO_2 at $T_{\text{substrate}} = 303$ K extracted from VASE measurements. Green dotted curve: UV–vis measurement of pentacene dissolved in dichlorobenzene. The energy axis is plotted to scale, but the ordinate axes are scaled arbitrarily with respect to $\Delta R/R$. Adapted with permission.^[62] Copyright 2011, American Physical Society.

to as “free exciton” feature in the literature,^[66–72] is close to the absorption peak dubbed “a” in Figure 7 and increases strongly with reducing temperatures.^[68,70–72] The strong temperature dependence of PL is typically governed by recombination processes into either radiative or non-radiative states. For example, below a temperature of 250 K, often several new pentacene transitions appear in the band gap region, which are understood to originate from self-trapped excitons (STE) due to local defects.^[66,70,72] Indeed, STE are absent in high-quality ML domains of pentacene,^[69] whereas these features are about as intense as the “free exciton” line in few-nanometer-thick pentacene films at certain temperatures.^[72] This demonstrates that PL is extraordinarily sensitive to trap states, and knowledge thereof may be important for the understanding of the energy

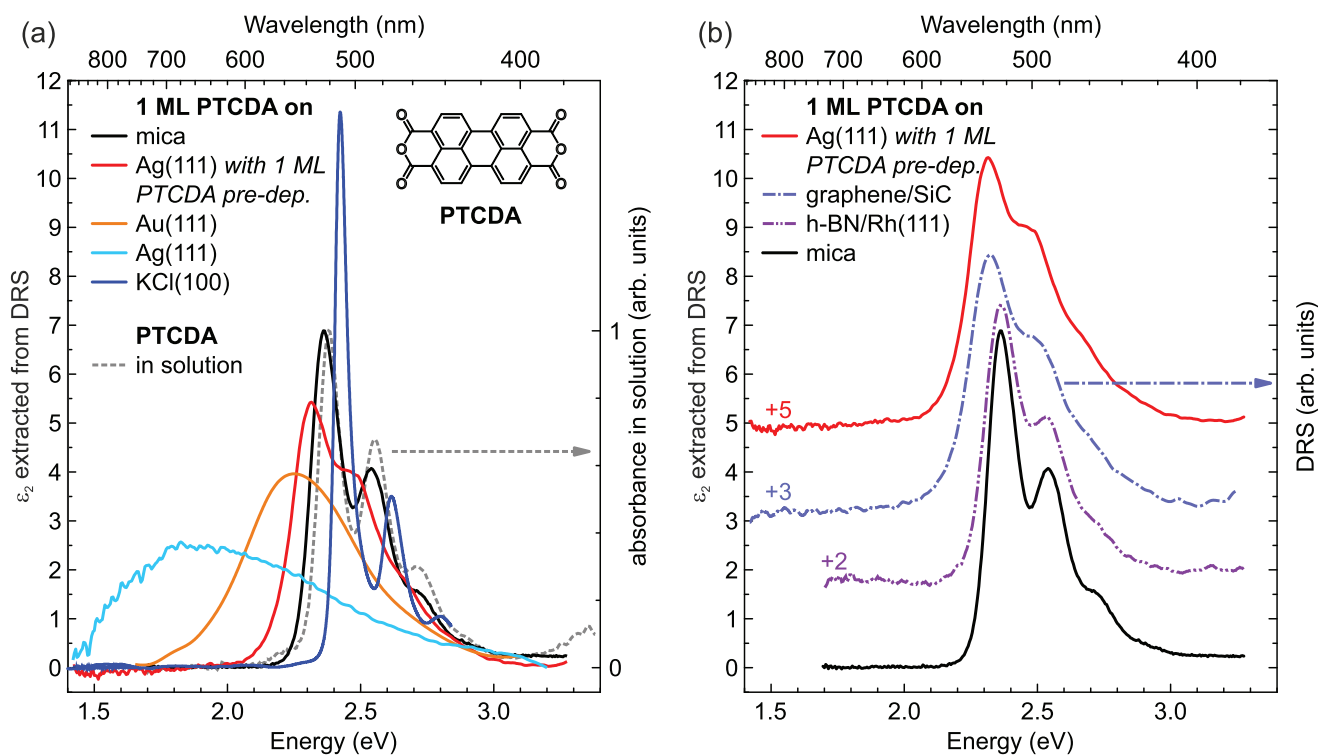


Figure 8. Imaginary parts, ϵ_2 , of the dielectric functions of a monolayer of PTCDA on various substrates. a) PTCDA on mica,^[61] on Ag(111) covered with a predeposited PTCDA monolayer,^[61] on Au(111),^[77] on Ag(111),^[61] and on KCl(100) extracted from DRS data.^[78] As a reference spectrum for monomeric behavior, the normalized absorbance of PTCDA in dimethyl sulfoxide (DMSO, dashed line) is shown.^[79] b) PTCDA on h-BN/Rh(111)^[80] and DRS data of PTCDA on graphene/SiC^[81] shown in comparison to the first two substrates in (a). The spectra in (b) are vertically shifted for clarity. The arrows point to the corresponding ordinate.

level alignment.^[73] A significant drawback compared with DRS is that PL signals may become quenched for ultrathin films, for example, due to non-radiative recombination directly at the adsorbate–substrate interface or due to energy transfer with nearby metal surfaces.^[70,74,75]

While in the above example the measured DRS signals can be directly interpreted in terms of the light absorption behavior of the molecules, this is not generally the case because of complicated dependencies of the signal on the optical functions of the involved materials, including the substrate.^[76] This makes a quantitative analysis of such spectra more complicated, insofar as the direct comparison of DRS spectra obtained for different substrates is often not very revealing. One should therefore extract the optical functions of the adsorbed thin film (e.g., the dielectric function $\epsilon = \epsilon_1 - i\epsilon_2$, with ϵ_1 and ϵ_2 being the real and imaginary parts, respectively) from the DRS signal using a numerical approach.^[53]

The imaginary parts ϵ_2 of the dielectric functions of a ML of PTCDA on different substrates are exemplarily shown in **Figure 8**. It can be seen that the spectral signatures of PTCDA on i) inert mica, ii) the Ag(111) surface covered with a predeposited PTCDA ML, iii) Au(111), and iv) Ag(111) exhibit a clear tendency, namely to red-shift and to experience additional broadening from (i) to (iv) due to an increasing electronic interaction with the substrate; an effect which is often dubbed hybridization of the molecules with the substrate.^[61] In fact, for PTCDA on Ag(111) a partial charge transfer into the former

LUMO was found by means of PES and electron energy loss spectroscopy.^[82–86] This demonstrates that DRS can help not only to distinguish between the two extreme cases of weak and strong electronic interaction (often referred to as physisorption and chemisorption in the literature, respectively) but also fine nuances in between. The latter is illustrated in **Figure 8b**, where in addition to (i) and (ii), the spectra of a PTCDA ML on epitaxial graphene/SiC^[81] and on hexagonal boron nitride (h-BN)/Rh(111)^[80] form a spectral series that suggests a hierarchy. In fact, we expect the adsorbate–substrate coupling to increase in the following order: mica (bulk insulator), h-BN (wide-gap 2D-material), graphene ([close to] zero-gap 2D-material), and PTCDA wetting layer (hybridized with a Ag(111) substrate). If a charge transfer, however, is effectively integer, characteristic spectral features of the respective ionic species (e.g., monoanions or dianions) can be observed.^[15,20,87,88]

For the analysis of optical spectra, structural circumstances may play an important role. For instance, a ML of PTCDA on KCl(100) shows very narrow absorption features (cf. **Figure 8a**), typically only observed for optical spectroscopy at low temperatures. This indicates that inhomogeneous broadening is strongly reduced compared to other substrates originating from a commensurate brick-wall instead of herringbone packing.^[78]

To sum up this section, it was shown that optical spectroscopy techniques reach submonolayer sensitivity for thin molecular films with spectral resolutions sufficient to observe vibronic substructures. The electronic adsorbate–substrate

interaction strength and also structural information can be deduced to a certain extent (e.g., flat-lying vs upright-standing molecules and brick-wall vs herringbone packing). From the manifold optical absorption spectroscopies, DRS in particular is very suitable to be performed in situ and is applicable to almost any sort of substrate making this technique a versatile tool to complement the electron spectroscopy techniques discussed here.

2.4. Two-Photon Photoemission Spectroscopy

In 2PPE spectroscopy, two laser pulses (often called “pump photons” and “probe photons”) are used to excite and eject electrons from a sample with subsequent detection in an electron energy analyzer similarly used in (angle-resolved) UPS measurements, cf. **Figure 9**.^[89] Both pulses are separately adjustable, often employing frequency doubling or tripling, with tunable photon energies in the visible and near UV range. A delay stage allows for a variable time delay, Δt , of both pulses at the sample. Usually, but not mandatorily, the energy of the first photon $\hbar\omega_1$ is chosen to be smaller than the work function of the sample, so that single-photon photoemission is prohibited. Instead, $\hbar\omega_1$ excites the sample via an unoccupied molecular orbital, an unoccupied substrate band, an image potential state (IPS), or even a virtual intermediate state. The second photon with

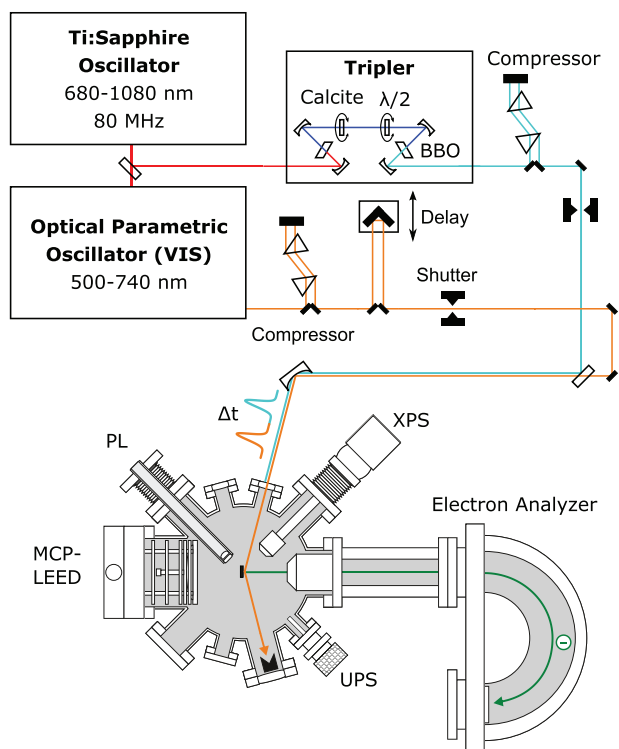


Figure 9. Typical setup for 2PPE experiments. The two photon beams, whose energies can be varied, are formed outside the vacuum chamber. They irradiate the sample (inside the vacuum chamber) at the same position, but with an adjustable time delay, Δt . A hemispherical electron energy analyzer is frequently employed, similar to (angle-resolved) UPS measurements. Reproduced with permission.^[89] Copyright 2018, IOP Publishing.

the energy $\hbar\omega_2$ then leads to the emission of an electron whose energy (and momentum) can be recorded in situ as sketched in **Figure 9**. Due to the typical pulse widths of ≈ 100 fs and the variation of Δt , time-resolved measurements are feasible. The highest electron emission intensity of a given feature occurs if both photons arrive simultaneously at the sample ($\Delta t = 0$). This intensity subsequently decreases as a consequence of the finite lifetime of the intermediate state and a diminished population thereof probed by a delayed second photon. Several two-step processes can occur in 2PPE, some of which are illustrated in **Figure 1**. The 2PPE technique, its theoretical backgrounds, recent progress, and applications have been already reviewed in the literature.^[90–93]

The experimental results summarized in **Figure 10** focus on stacked, homoepitaxially, and heteroepitaxially grown planar junctions of PTCDA and CuPc on Ag(111).^[89] The 2PPE spectra shown there were recorded with $\hbar\omega_{\text{vis}} = 2.00$ eV and $\hbar\omega_{\text{UV}} = 4.64$ eV, whereas the work functions of the samples had previously been reported as $\Phi_{\text{Ag(111)}} = 4.8$ eV and $\Phi_{\text{PTCDA/Ag(111)}} = 4.9$ eV.^[83] The microscopic structures of I) PTCDA/Ag(111), II) PTCDA/PTCDA/Ag(111), as well as III) CuPc/PTCDA/Ag(111) were thoroughly characterized by combining low-energy electron diffraction, scanning tunneling microscopy, and other methods.^[83,94–96] To recapitulate the main structural findings, the molecules in all three systems, (I)–(III), are aligned parallel to the substrate surface and form densely packed, commensurate overlayers with respect to Ag(111). The first and second MLs of PTCDA on Ag(111) each have identical two-molecule unit cells with a 2D herringbone (HB) arrangement, while a rigid lateral displacement is observed between molecules in adjacent layers.^[83,94,95] The CuPc unit cell contains six molecules and exhibits a commensurate registry with the underlying PTCDA ML.^[96] Consequently, these highly ordered thin films represent ideal model systems for the study of electronic properties without significant inhomogeneous broadening effects.

Lerch et al. assigned the discernible features in **Figure 10a** based on systematic variations of either $\hbar\omega_{\text{vis}}$ or $\hbar\omega_{\text{UV}}$, which yields different final-state energy variations for the main features H and L2 attributed to the CuPc HOMO and LUMO+2, respectively.^[89] Their assignment was further assisted by the dispersion relations of the features as extracted from 2PPE spectra for a variety of azimuth angles. The series of IPSs ($n = 1, n = 2$) as well as the interface state all exhibit parabolic dispersions, whereas H and L2 lack any distinguishable sign of angular dependence, as expected for essentially non-interacting orbitals of flat-lying molecules. The specific CuPc orbitals involved in the probe process were concluded from energetic arguments: UPS experiments for the same system (III) yielded a HOMO-derived peak with its maximum at ≈ 0.9 eV below E_F ,^[96] and VUV-IPES results indicated a LUMO+2-derived peak with its maximum at ≈ 5.0 eV above the HOMO (albeit for a much thicker film $d_{\text{CuPc}} \approx 10\text{--}20$ ML directly on Ag(111)).^[98] Thus, the expected energy range of the LUMO+2-derived feature is ≈ 4.1 eV above E_F , which is indeed the case for the analyzed L2 feature.^[89] It is worth noting that the 2PPE data by Lerch et al. revealed no clear indication of the CuPc LUMO or the LUMO+1. Their assignment of the L2 feature to the LUMO+2 relies strongly on earlier VUV-IPES results,^[98] while NUV-IPES

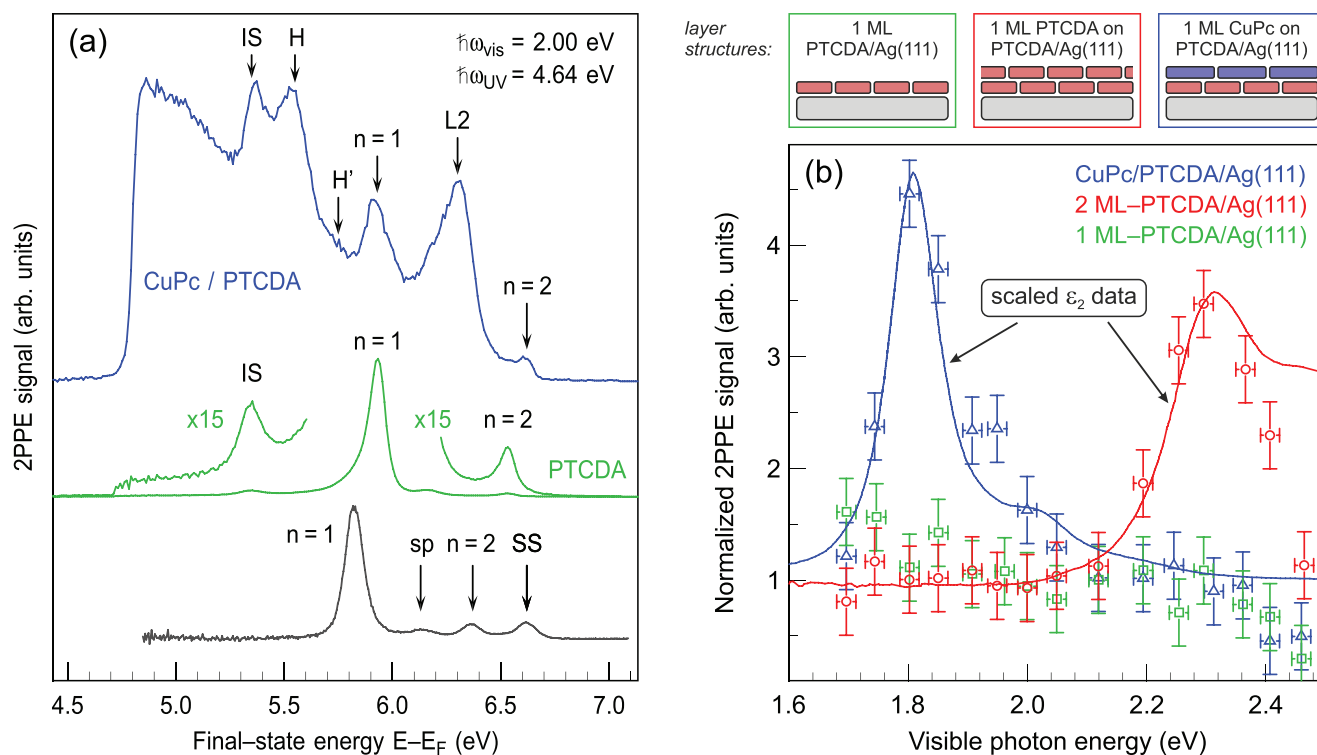


Figure 10. a) Experimental 2PPE results for a pristine Ag(111) substrate (black curve), PTCDA/Ag(111) (green curve), and CuPc/PTCDA/Ag(111) (blue curve). PTCDA and CuPc molecular layers have a thickness of 1 ML each. Pump and probe photon energies are given in the inset, the time delay is $\Delta t = 0$. The spectra are plotted on the “final-state” energy scale, that is, the energy of the photoelectrons with respect to the silver Fermi energy (usually, the reference is set to $E_F = 0$). The discernible features were identified by Lerch et al. as the Shockley surface state (SS) of Ag(111), a weak signature of the silver sp-band (sp), and a series of image potential states ($n = 1, 2$) that change slightly upon molecular adsorption. Additionally, an interface state (IS) and several features ascribed to CuPc (H, H', L2) are labeled, see the text for details. b) Interface state 2PPE intensity (open symbols) plotted versus $\hbar\omega_{\text{vis}}$ for CuPc/PTCDA/Ag(111) and PTCDA/PTCDA/Ag(111) in comparison to PTCDA/Ag(111); the respective layer structures are sketched in the upper panels. While in the latter case the IS intensity shows no significant variation, in the former two cases it depends on the photon energy. The additional curves are the scaled imaginary parts, ϵ_2 , of the dielectric functions of CuPc (blue) and PTCDA (red), extracted from DRS measurements both with 1 ML PTCDA/Ag(111) as the reference substrate.^[61,97] Adapted with permission.^[89] Copyright 2018, IOP Publishing.

(i.e., LEIPS) data for system (III) are currently not available to the best of our knowledge. There are, however, NUV-IPES measurements for CuPc several nanometers thick on indium tin oxide (ITO) substrates using five different optical bandpass energies from 2.86 to 4.97 eV.^[36] Comparing different substrates is not necessarily an unsurmountable obstacle, because in both cited papers the nominal CuPc film thicknesses were in the order of 10 nm.^[36,98] Bearing in mind the small mean free path of electrons in organic solids,^[99] those spectra stem from the uppermost organic layers and should therefore not be significantly influenced by charge transfer with the respective substrate. The energy alignment of the unoccupied levels with the Fermi energy, however, may depend on the specific substrate because of different molecular orientations (cf. Figure 5), and in fact CuPc adsorbs flat-lying on Ag(111)^[100,101] but almost upright-standing on ITO.^[102,103] Furthermore, we compare energies of the LUMO, LUMO+1, and LUMO+2 of CuPc calculated by means of density functional theory (DFT) for a freestanding film^[104] and for a free molecule^[105] using the same screened hybrid functional by Heyd, Scuseria, and Ernzerhof (HSE). These values are compiled in Table 1.

Because of the good agreement of the relative energies, the association of the L2 feature with the LUMO+2 in the 2PPE

data of Lerch et al. seems justified.^[89] Nevertheless, the assignment is not straightforward, and it has been demonstrated that especially the DFT results for CuPc depend strongly on the employed functional, with inferior performance of semi-local functionals.^[104,105] Therefore, although the L2 feature was plausibly assigned to the LUMO+2,^[89] such an identification can be laborious, especially when crucial reference data is missing (such as the lack of LUMO-derived and LUMO+1-derived features in the 2PPE data). In summary, the experimental spectroscopic information for the lowest unoccupied levels of the heteromolecular system CuPc/PTCDA/Ag(111)—although exceptionally well characterized in the literature^[89,96,97,106–108]—is only indirectly accessible via comparison to data for related (but not identical) systems or through theoretical calculations. The fact that vital spectroscopic data for CuPc/PTCDA/Ag(111) are still missing requires one to imply the energetic position of the LUMO-derived level, thus leaving uncertainty in the discussion of the transport levels.

An interesting aspect of the comparison between 2PPE and optical spectroscopy is provided in Figure 10b. The plot depicts the photoelectron intensity of the interface state feature, which was shown to be pumped by the photons in the visible spectral range and probed by $\hbar\omega_{\text{UV}}$.^[89] The data for CuPc/PTCDA/Ag(111)

Table 1. Experimental IPES data, given as peak maximum energies in electronvolt above E_F , for CuPc thin films in comparison to DFT-calculated values.

Reference	System	Method	LUMO	LUMO+1	LUMO+2
Krause et al. ^[98]	CuPc on Ag(111)	VUV-IPES	1.51	2.30 ^{a)}	3.43
Yoshida ^[36]	CuPc on ITO	NUV-IPES (LEIPS)	1.91 ^{b)}	n/a	3.91 ^{b)}
Lüftner et al. ^[104]	Freestanding CuPc film ^{c)}	DFT (HSE functional)	1.74	2.55	n/a
Marom et al. ^[105]	Free CuPc molecule ^{d)}	DFT (HSE functional)	1.80	2.66	3.50

^{a)}Very weak, unrecognizable feature, deconvoluted via Gaussian peak fitting of the data; ^{b)}Assignments were not given in the original source. Peaks are labeled here based on their similarity to the spectra on Ag(111) in accordance with an unrecognizable LUMO+1 feature; ^{c)}Values are given relative to the HOMO, which coincides with E_F ; ^{d)}Values are given relative to the HOMO.

and for PTCDA/PTCDA/Ag(111) clearly depend on $\hbar\omega_{\text{vis}}$ and compare favorably with ϵ_2 data of the same systems extracted from earlier DRS measurements.^[61,97] Lerch et al. concluded that the population of the interface state originates from optically excited molecules in the respective second layer, while the chemisorbed first PTCDA ML couples so strongly to the Ag(111) substrate that it does not yield a resonant excitation of the interface state.^[89]

3. Consistent Interpretation of Complementary Spectroscopic Techniques

We argued in the preceding section that the available spectroscopic data of a given system are often insufficient, even in cases where an abundance of literature reports exists, such as for CuPc/PTCDA/Ag(111). For some systems, like pentacene thin films, the database is in fact more extensive and yields that the energy alignments of the occupied and unoccupied bands depend rather sensitively on the physical structure formed, for example, face-on oriented versus edge-on oriented molecules. Those microscopic structures may be influenced by the substrate, the deposition parameters (e.g., substrate temperature, molecular flux), post-growth treatments (e.g., annealing), or they may even differ between the first organic layer and multilayer samples. Moreover, molecular aggregation can lead to the formation of energy bands with sizeable dispersion (even in cases where the electronic adsorbate–substrate coupling is minor), adding to the complexity of the respective spectra. Given all these circumstances, it is useful to systematize the experimental data of molecular aggregates and to understand how they are related to the respective molecules in the gas phase (i.e., monomers). As a guide for this endeavor, a recently introduced notation shall be summarized and employed in the following.

3.1. Conceptual Framework of Energy Level Diagrams

In this section we lay out the concepts of drawing accurate energy level diagrams brought forward in the literature.^[17,24] This model was developed for the often encountered case of weak molecule–substrate interaction, and excludes hybridization, or, in other words, fractional charge transfer.

A noticeable distinction between inorganic semiconductor crystals and molecular aggregates stems from the usually much smaller electronic bandwidths of the latter. Photoemission

(inverse photoemission) spectroscopy experiments, for example, obviously involve an electron detachment (attachment) process and thus a positively (negatively) charged final state of the probed molecule. Since this charge possesses a localized character for organic molecules, especially in the frequently encountered case of weak environmental interactions, on-site Coulomb energies play a decisive role in the rationalization of the experimental results. One may speak of charging energies E_C^+ and E_C^- of the positively and negatively charged molecule, respectively, and they are related to the on-site Coulomb energy U (via $U = E_C^+ + E_C^-$) in the Hubbard model, with typical energies being in the order of several eV.^[109–111] Considering, for example, the photoemission (cf. UPS in Figure 1) from a single gas-phase molecule in the ground state (S_0), it is clear that the emitted electron interacts via Coulomb attraction with the photohole remaining on the molecule, which itself is then in the cationic state. Therefore, the observed kinetic energy of the photoelectron is reduced by E_C^+ . Conversely, the probe process 2PPE(3) illustrated in Figure 1 denotes the emission of a photoelectron from an anionic molecule. In this case, the detected kinetic energy of the photoelectron is increased by E_C^- due to Coulomb repulsion of the excess electron. Such probe processes constitute a considerable perturbation of the N -electron system of the molecule, which is why these techniques do not measure the energy levels of unperturbed molecules in their ground state. Instead, the initial and final states of the spectroscopic probe processes require proper consideration, and it was suggested to express this as $\text{LEVEL}_{\text{initial state}}^{\text{final state}}$.^[17] Hereby, “LEVEL” stands for the molecular orbital which is most decisively involved in the probe process. The subscript (superscript) explicitly designates the initial state (final state) of the probe process, where “0” denotes the neutral ground state, “+1” the cationic state, “–1” the anionic state, and “0*” an electronically excited state (S_1) of a neutral molecule. For example, a spectroscopic feature related to the HOMO of a given molecule examined via UPS is represented by H_0^+ , while a LUMO-related feature stemming from a 2PPE(3) process is dubbed L_{-1}^0 in this notation. We point out that L_{-1}^0 (as in 2PPE(3)) or in anion photoelectron spectroscopy^{[112])} and L_0^- (as in IPES) features are expected to have the same energy according to our previously introduced model,^[17] because the respective probe processes involve the same states, just with reversed roles. Various other examples are listed in Figure 1. Using this notation, we can express the experimentally determined ionization energy as $\text{IE} = E_{\text{vac}} - H_0^+$ and the electron affinity as $\text{EA} = E_{\text{vac}} - L_{-1}^0 = E_{\text{vac}} - L_0^-$ depending on the employed method.

The next logical step for our discussion is to consider molecules adsorbed on a surface and/or embedded in a dielectric medium. In those cases, charged molecules (either in the initial state or in the final state) interact with their polarizable environment depending on the dielectric properties of the materials and on the location of the charges within the film structure (differences may occur for molecules in the wetting layer, within a multilayer, or in the topmost layer toward the vacuum, for example).^[113,114] Thereby, charges are screened, and the polarization acts on cationic and anionic states as a stabilizing effect. The corresponding polarization energies P^+ and P^- thus counteract the charging energies E_C^+ and E_C^- , and in the extreme case of very high environmental polarizability they can even achieve cancellation. Additional contributions to P^+ and P^- may come from permanent dipole or multipole moments if present.^[115] Further phenomena, such as time-dependent polaronic effects, may influence the polarization energies but are beyond the scope of this article. For our discussion, we assume that electronic rearrangements occur during relevant spectroscopic processes, while the geometry of the molecular framework (i.e., the coordinates of the nuclei) remains fixed. Typical time scales of photoionizations are in the order of 10^{-15} – 10^{-16} s, for example, which is why only vertical transitions are generally regarded here.^[116]

Furthermore, molecular adsorbates are subject to van der Waals interactions and possibly also to electrostatic interactions via permanent dipoles or multipoles (we exclude chemisorbed molecules from our discussion). Consequentially, the associated adsorption and condensation energies lead to a shift of the measured levels toward lower energies with respect to a gas-phase molecule. In the picture of molecular orbitals, each level may in principle exhibit a different shift, which can be expressed as individual quantities, w . The conjugated organic molecules discussed here are characterized by delocalized wave functions of the frontier orbitals, and since the spatial extents of the HOMO and the LUMO are typically similar it is reasonable to assume that $w(\text{HOMO}) \approx w(\text{LUMO})$. Hence, in an energy level diagram the frontier orbitals of an adsorbed molecule are expected to shift downward by a similar amount, w , with respect to a gas-phase molecule.^[17,24]

Finally, optical transitions such as the $(\text{H} \rightarrow \text{L})_0^{0*}$ absorption process are taken into account for this model. This notation can be used if the optical excitation is dominated by a HOMO \rightarrow LUMO transition in the single-particle picture, which is reasonably fulfilled in many cases. In the states picture, the absorption process is adequately described as an $S_0 \rightarrow S_1$ transition, where the difference between the excited (S_1) and the ground state (S_0) equals E_{opt} . The optical absorption process is further accompanied by an electronic relaxation of the excited state, which yields a downward energy shift of $-E_{\text{rel}}^{\text{exc}}$ in an energy level scheme. This term does not include the geometric relaxation of the molecular framework, as the coordinates of the nuclei are considered fixed on the time scales of the relevant spectroscopic processes (see above).

In case a positively charged state is involved in the probe process, it is possible to summarize the shift of each energy level with respect to an unperturbed molecule in the gas phase as

$$\Delta E_{\text{pos}} = -(E_C^+ - P^+) - w - E_{\text{rel}}^{\text{exc}} \quad (2)$$

Conversely, if a negatively charged state is part of the probe process, then the shift can be expressed as

$$\Delta E_{\text{neg}} = +(E_C^- - P^-) - w - E_{\text{rel}}^{\text{exc}} \quad (3)$$

In both cases, of course, the excited state relaxation energy, $E_{\text{rel}}^{\text{exc}}$, applies only if an excited molecular state occurs in the probe process. Since $E_{\text{rel}}^{\text{exc}}$ is expected to be rather small, it is sometimes neglected for the sake of simplicity.^[17,24] In addition, the terms w , P^+ , and P^- apply to molecular films, but they are negligible for molecules in the gas phase.

The above considerations are summarized in **Figure 11**, where the discussed quantities are represented in the states picture and in the energy levels picture for a molecule in the gas phase compared to the same molecule adsorbed on a substrate.

For electronic and optoelectronic devices, the transport gap, $E_{\text{trans}} = L_0^{-1} - H_0^{+1}$, and the optical gap, $E_{\text{opt}} = L_0^{0*} - H_0$, are very important quantities. Their difference defines the exciton binding energy, $E_B = E_{\text{trans}} - E_{\text{opt}}$, as another key parameter, especially for light-emitting or light-harvesting electronic applications.

Next, we will put into practice the above thoughts to the extensively investigated molecule pentacene and thin films thereof on weakly interacting substrates.

3.2. Application to Pentacene

3.2.1. The Role of Molecular Orientations

In the following, we aim at a quantitatively accurate visualization of the complementary spectroscopic information for pentacene in the gas phase compared to a thin pentacene film adsorbed on graphite.

Bearing in mind our discussion in Section 2, it is important to discriminate between different molecular orientations in pentacene thin films. As demonstrated by means of X-ray diffraction and atomic force microscopy, pentacene forms extended crystalline domains of essentially flat-lying molecules on HOPG, cf. Figure 3.^[35] There, the long molecular axis is oriented parallel to the graphite surface, and although the molecular plane is tilted around that axis this orientation is usually referred to as “face-on” or “lying.”^[30,40] By contrast, the orientation of pentacene films on SiO_2 , for example, is typically found to be “short-edge-on” (also called “end-on” or “standing”) except for particular growth conditions at lower temperatures.^[65] The standing pentacene films exhibit different spectra (see the UPS, LEIPS, and DRS data in Section 2, for instance) than their lying counterparts, and we will now focus on the latter. Thereby, we compare pentacene data for similar nominal film thicknesses of about 1 ML (here 1 ML denotes a single face-on oriented pentacene layer fully covering a surface), where the physical thickness of a single molecular layer was reported to be 0.37 nm.^[35] Given that the observed HOMO-derived band dispersion primarily occurs in the direction perpendicular to the graphite surface (k_{\perp}),^[35] it should be absent in ML samples of face-on oriented pentacene on graphite. The spectrum depicted in Figure 2b corroborates this statement, because of the visible vibronic substructure.^[30]

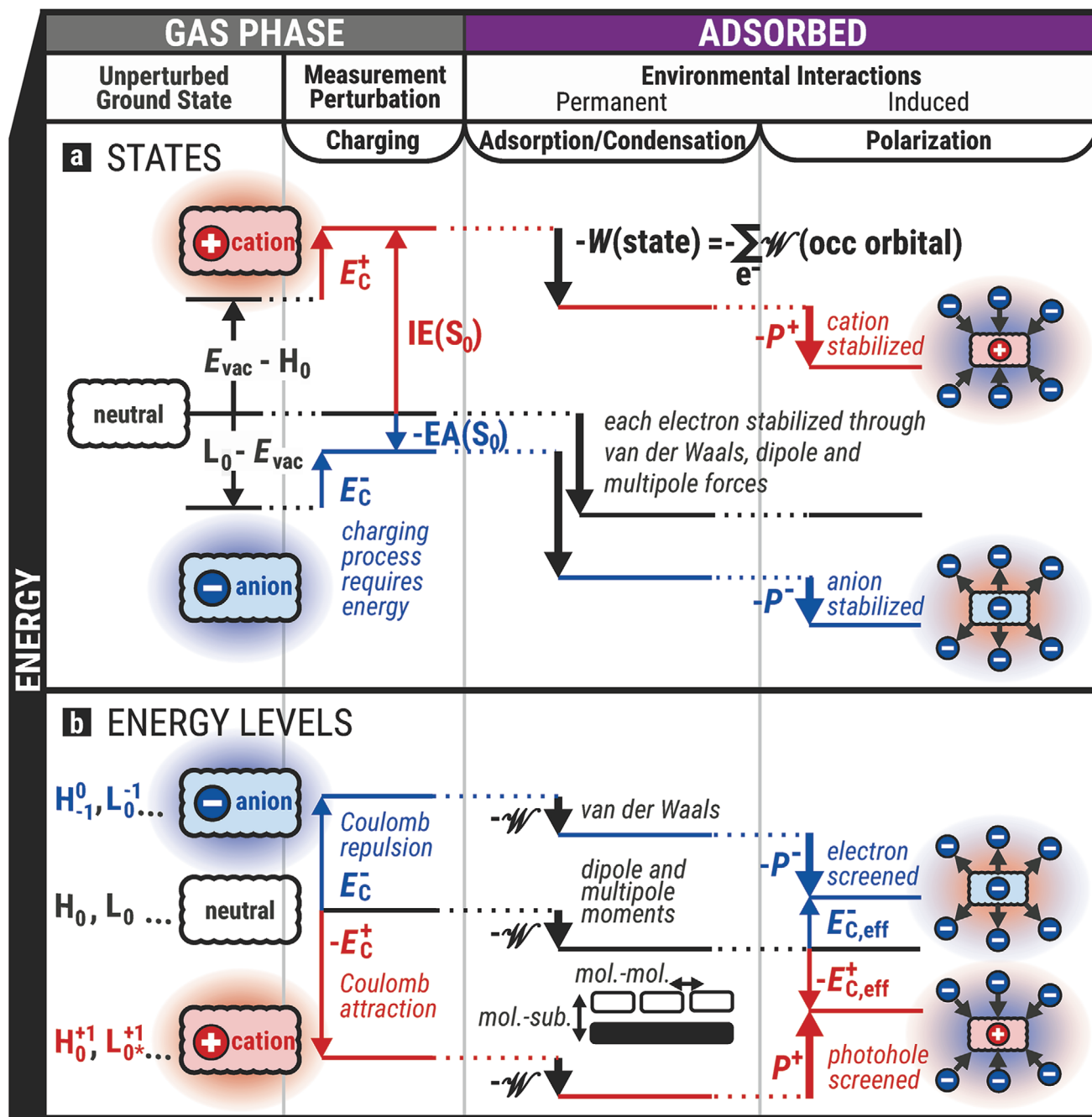


Figure 11. Schematic overview of the influence of measurement perturbations as well as permanent and induced environmental interactions for a given molecule represented by a black contour line. a,b) These effects are depicted in a multiparticle state diagram (a) as well as in a single-particle energy level diagram (b) for comparison. See the text for details. Reproduced with permission.^[17] Copyright 2019, Royal Society of Chemistry.

3.2.2. Comparison of Complementary Spectroscopic Results

Owing to the wealth of available data in the literature, we first give an overview of experimental data for pentacene in Table 2. Subsequently, we will comment on these values in more detail and compare them to related data reported by others.

The vertical ionization energy of PEN in the gas phase was measured by Coropceanu et al. as $IE(S_0) = 6.589$ eV.^[32] Kera and Ueno pointed out that the reported spectrum shows a

high-kinetic-energy shoulder (cf. Figure 2a) and attributed this to a possible instrumental artifact. Since this shoulder is absent in the measurement by Kera and Ueno, we adopt their value of $IE(S_0) = 6.61$ eV.^[30] Nonetheless, both values are similar and compare favorably with other reported experimental data (Neaton et al.:^[118,119] 6.63 eV; Dabestani and Ivanov:^[120] 6.61 eV) as well as theoretical results (Li et al.:^[121] 6.55 eV, obtained with eigenvalue-only self-consistent GW calculations [eVGW]).

Table 2. Experimental data, given as peak maximum energies (unless otherwise noted) for pentacene (PEN) in the gas phase and in face-on adsorbed molecular layers (for brevity, IE and EA are defined relative to $E_{\text{vac}} = 0$ here).

Reference	System	Method	Assignment	Comment	Energy [eV]
Kera and Ueno ^[30]	PEN (gas phase)	UPS at 433 K	IE(S_0) $\equiv -H_0^{-1}$	Vertical IE	6.61
Masubuchi et al. ^[112]	PEN (gas phase)	Anion PES ^{a)}	EA(S_0) $\equiv -L_{-1}^0$	Vertical EA	1.43
Halasinski et al. ^[117]	PEN (gas phase)	MIS ^{b)} in Ne, Ar, and Kr	($H \rightarrow L$) $_0^0$	Extrapolated ^{c)}	2.31
Kera and Ueno ^[30]	1 ML PEN/HOPG	UPS at 295 K	IE(S_0) $\equiv -H_0^{-1}$	Face-on	5.68
Yoshida et al. ^[40]	0.5 nm PEN/HOPG ^{d)}	NUV-IPES (LEIPS)	EA(S_0) $\equiv -L_0^{-1}$	Face-on	2.64
Zhang et al. ^[60]	PEN on α -Al ₂ O ₃	DRS	($H \rightarrow L$) $_0^0$	Face-on	2.13
Yoshida et al. ^[40]	0.5 nm PEN/HOPG ^{e)}	NUV-IPES (LEIPS)	$\Phi = E_{\text{vac}} - E_{\text{F}}$	Via dI_{sample}/dE	4.57

^{a)}Pentacene anions (PEN⁻) are produced through electron attachment and mass-selected in combination with a time-of-flight mass spectrometer. PEN⁻ is irradiated with laser light, and the kinetic energy of the emitted photoelectrons is analyzed; ^{b)}Matrix isolation spectroscopy (MIS) in cryogenic noble-gas condensates; ^{c)}Value for gas-phase PEN extrapolated and rounded, see the text for details; ^{d)}We fitted the original LEIPS data for $d_{\text{PEN}} = 0.5$ nm on HOPG using Gaussian peaks (on a linear + exponential background) and subtracted the first peak's maximum energy from E_{vac} ; ^{e)}We analyzed the original data of the first derivative of the sample current.

The vertical ionization energy of PEN in a face-on ML on HOPG was measured by Yamane et al. yielding IE(S_0) = 5.68 eV at 295 K, cf. Figure 2b.^[33] There, the vibronic substructure of the HOMO-derived feature is discernible.

The adiabatic electron affinity (AEA) of PEN in the gas phase was measured by Masubuchi et al. by means of anion photoelectron spectroscopy.^[112] To this end, pentacene anions (PEN⁻) are produced through electron attachment and mass-selected in combination with a time-of-flight mass spectrometer. PEN⁻ is then irradiated with laser light, and the kinetic energy of the emitted photoelectrons is analyzed. Due to the clearly resolved spectra showing the electronic transition and additional vibrational components, Masubuchi et al. concluded that the measured AEA should be equivalent to the vertical detachment energy (which is important because we only consider vertical transitions here). We thus adopt their measured value as vertical EA(S_0) = 1.43 eV.^[112] Similar experimental values (Neaton et al.:^[118,119] 1.39 eV; Crocker et al.:^[122] 1.35 eV) and theoretical values (Li et al.:^[121] 1.53 eV, obtained with evGW calculations) have been reported. For the spectroscopic process we note that, in principle, an L_{-1}^0 feature in anion PES is expected at the same energy as an L_0^{-1} feature in LEIPS according to the model proposed by us (see above).^[17] In that sense, anion PES is similar to the probe process in 2PPE(3), cf. Figure 1.

Yoshida et al. acquired LEIPS data for thin PEN films on HOPG.^[40] We fitted the spectrum for $d_{\text{PEN}} = 0.5$ nm using Gaussian peaks on a linear + exponential background. This was possible because the LEIPS data are digitally accessible without significant loss of quality (in the original publication they are contained as vector graphics). We obtain a value of EA(S_0) = 2.64 eV for the peak maximum, which is given here because we consider vertical transitions. Note that this value obviously differs from the peak onset given in Figure 5. The instrumental broadening of the LEIPS setup employed by Yoshida et al. is mainly determined by the energy spread, $\Delta E = 0.25$ eV, of the impinging electrons and the bandpass width of $\Delta E = 0.26$ eV (a bandpass with a center energy of 4.38 eV was used).^[36,40] Therefore, a possible vibronic substructure cannot be resolved (as discussed in Section 2.2), and we

assume here that the fitted peak position corresponds to a vertical transition.

Halasinski et al. measured the optical transition energies of individual PEN molecules embedded in cryogenic noble-gas matrices (Ne, Ar, Kr) with very high precision.^[117] From those results, one can extrapolate the transition energy for the free gas-phase molecule according to Rouillé et al.^[123] as follows:

$$E_{\text{gas phase}} = E_{\text{Ne matrix}} + (E_{\text{Ne matrix}} - E_{\text{Ar matrix}})/(R_\alpha - 1) \quad (4)$$

Here, $R_\alpha = 4.13$ is the ratio of the polarizabilities of Ar with respect to Ne.^[124] With $E_{\text{Ne matrix}} = 2.2845$ eV and $E_{\text{Ar matrix}} = 2.2149$ eV reported by Halasinski et al.^[117] one obtains $E_{\text{gas phase}} = 2.3068$ eV, which we adopt as the ($H \rightarrow L$) $_0^0$ value for gas-phase PEN.

Optical absorbance data for a face-on pentacene ML on graphitic substrates are not available to the best of our knowledge. Therefore, DRS data for PEN on α -Al₂O₃(0001) are employed here as a substitute, cf. Figure 7. Zhang et al. argued that the first PEN layer on α -Al₂O₃(0001) is flat-lying.^[60] The component labeled "c" in their DR spectra obtained at room temperature is found at $E = 2.13$ eV, and we adopt this as the ($H \rightarrow L$) $_0^0$ value for a face-on PEN ML on a weakly interacting substrate.

The work function, $\Phi = E_{\text{vac}} - E_{\text{F}}$, is usually measured by means of UPS or 2PPE via determination of the onset of the vacuum energy, that is, the secondary electron cutoff. For pristine graphitic surfaces, Φ is typically found in between 4.45 and 4.65 eV, depending on the surface quality as well as the cleaning/degassing procedure applied in vacuo.^[24] In a different approach, Φ can be extracted from the maximum of the first derivative of the sample current recorded during LEIPS measurements, cf. Figure 5. With this method, the experimental data by Yoshida et al. yield work functions of PEN on HOPG in the range between 4.53 and 4.57 eV for different pentacene film thicknesses.^[40] Therefore, we adopt a value of $\Phi = 4.57$ eV according to the data for 0.5 nm PEN/HOPG shown there.

In **Figure 12**, we depict the complementary spectroscopic data, using the values that we deem most reliable in the light of the above literature survey and discussion.

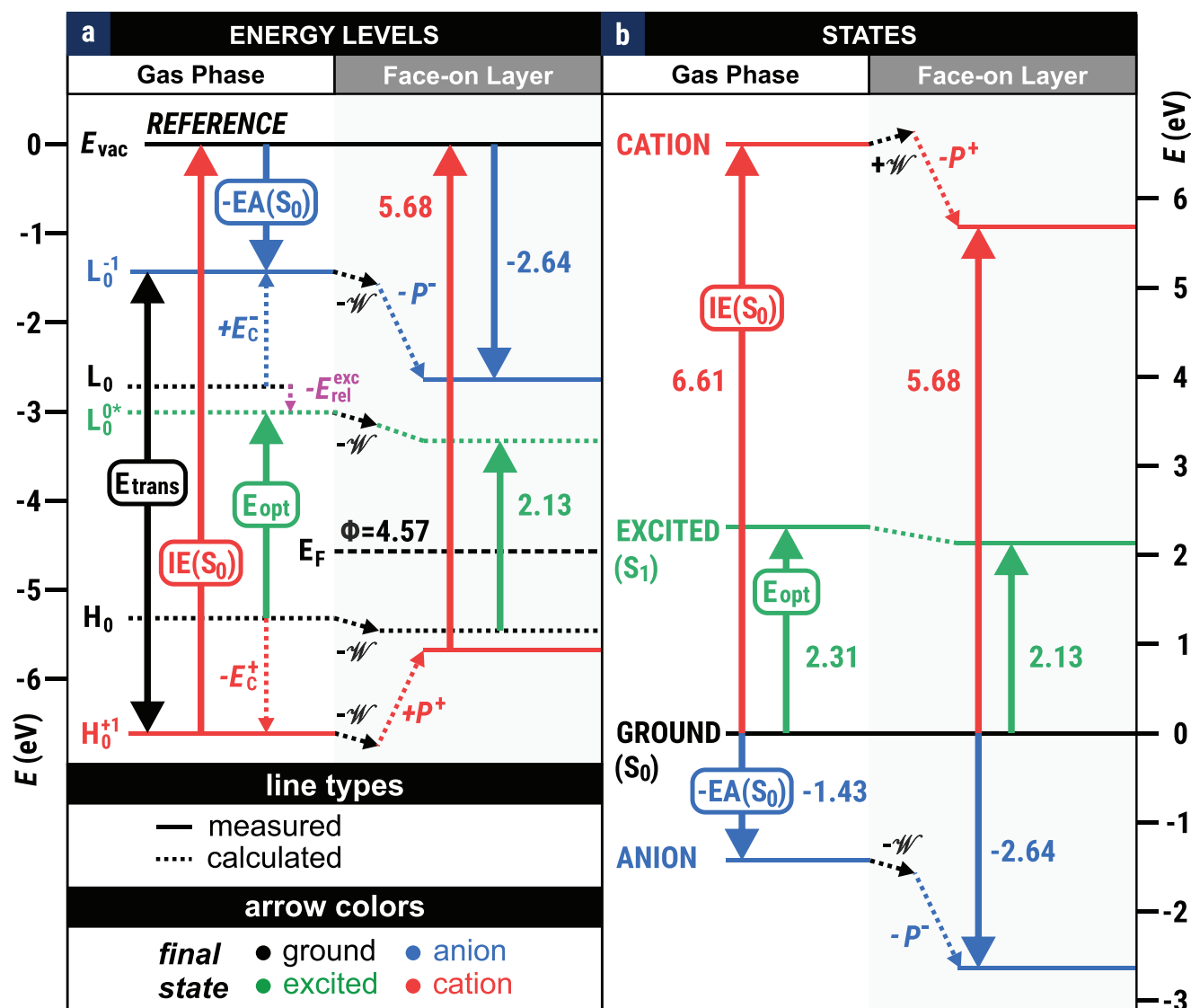


Figure 12. Graphical visualization of the data for pentacene listed in Table 2. a) Depicted as energy levels with the reference energy chosen as $E_{vac} = 0$. b) Depicted as molecular states with the S_0 ground state energy chosen as a point of reference. The energy unit of the ordinate axis is identical to panel (a) apart from the absolute position of the origin. Both (a) and (b) display data for gas-phase molecules as well as for face-on oriented pentacene adsorbed on weakly interacting substrates. The excited state relaxation energy, $E_{rel}^{exc} = 0.29$ eV, was obtained via calculations; see the text for details. The data are compiled in analogy to our previous work.^[24]

3.2.3. On the Symmetry of Charging and Polarization Energies

For the compilation of Figure 12, we made several assumptions, the most important ones being $E_c^+ = E_c^-$ and $P^+ = P^-$. For a rationalization of these crucial approximations, we invoke the causality principle: If the positive and negative charging energies are similar ($E_c^+ \approx E_c^-$), then the same holds true for the positive and negative polarization energies of those charges in a polarizable environment ($P^+ \approx P^-$).

On closer inspection, if the electronic distributions of the HOMO and the LUMO of a given molecule exhibit similar spatial extents (i.e., similar volumes), then the conformity of the charging energies $E_c^+ \approx E_c^-$ and hence of the polarization energies $P^+ \approx P^-$ are plausible consequences. For the same reason, we assume that $w(\text{HOMO}) \approx w(\text{LUMO})$, see

Section 3.1. We corroborated these approximations by means of DFT calculations as described in detail elsewhere.^[24] For the sake of the argument, we will briefly outline those computations here. The DFT calculations were performed employing the B3LYP functional and the 6-311G++(d,p) basis set. The geometry of the gas-phase molecule in the ground state was optimized, and the coordinates of the nuclei were kept fixed for subsequent calculations. We further employed a polarizable continuum model in the integral equation formalism,^[125] which is tantamount to placing a single molecule in a cavity of a dielectric medium with a relative permittivity, ϵ_r . While $\epsilon_r = 1$ obviously represents the situation of a single molecule surrounded by vacuum, we demonstrated previously that for a large variety of molecules $\epsilon_r \approx 3$ is a suitable choice to mimic the effective dielectric constant for a molecular ML adsorbed

Table 3. Theoretical results for pentacene in the gas phase and for a monolayer adsorbed flat-lying on graphite, compared to the main experimental results as depicted in Figure 12. All energies are given in eV.

Reference	System	E_{trans}	E_{opt}	E_{B}	E_{C}^+	E_{C}^-	$E_{\text{rel}}^{\text{exc}}$	P^+	P^-	ω
Figure 12	Gas-phase PEN	5.18	2.31	2.87	1.29 ^{a)}	1.29 ^{a)}	0.29 ^{b)}	0.00	0.00	0.00
Figure 12	1 ML PEN/graphite	3.04	2.13 ^{c)}	0.91	—	—	—	1.07 ^{d)}	1.07 ^{d)}	0.14 ^{e)}
Kirchhübel et al. ^[24]	Gas-phase PEN ^{f)}	4.76	1.90	2.86	1.29	1.28	0.29	—	—	—
Kirchhübel et al. ^[24]	PEN in a polarizable medium ^{g)}	2.77	—	—	—	—	—	0.95	1.03	—
Neaton et al. ^[118]	Face-on PEN/graphite ^{h)}	2.88	—	—	—	—	—	1.18	1.18	—
Yanagisawa ^[126]	5 ML PEN/HOPG ⁱ⁾	2.99	—	—	—	—	—	1.06	1.15	—

^{a)}In Figure 12, we assumed $E_{\text{C}}^+ = E_{\text{C}}^-$; ^{b)}The calculated value, $E_{\text{rel}}^{\text{exc}}$, for gas-phase PEN was employed. It is obtained through $E_{\text{rel}}^{\text{exc}} = L_0 - H_0 - E_{\text{opt}}$, with L_0 and H_0 computed via DFT, and E_{opt} computed via TD-DFT^[17]; ^{c)}For E_{opt} , we used the experimental data of PEN/ α -Al₂O₃(0001) in Figure 12; ^{d)}In Figure 12, we assumed $P^+ = P^-$; ^{e)}In Figure 12, we assumed ω to have the same value for all levels. It can be obtained via $\omega = \text{EA}(\text{adsorbed}) - \text{EA}(\text{gas phase}) - P^- = -(\text{IE}(\text{gas phase}) - \text{IE}(\text{adsorbed}) - P^+)$; ^{f)}In our previous report,^[24] only some of the quantities listed here were explicitly provided. The calculation result for the transition with $E_{\text{opt}} = 1.90$ eV yielded a much smaller oscillator strength than for another transition at 4.24 eV. This is in accordance with Figure 7 (bottom), where the corresponding experimental peaks labeled “c” and “e” differ markedly in intensity; ^{g)}Computed results for pentacene in a polarizable medium with the relative permittivity of $\epsilon_r = 3.05$ (see the text for details) to mimic the effective dielectric constant suitable for a molecular monolayer adsorbed on graphite; ^{h)}Based on the GW formalism using a polarization model for single pentacene molecules adsorbed on graphite; ⁱ⁾Based on the evGW formalism using a 5 ML slab of face-on PEN on graphite.

on graphite.^[24] With this formalism, we calculated the total self-consistent field energies of the molecules in different states, that is, neutral ground states, cations, anions, and the S₁ excited states (for the geometry of the neutral molecule). The latter were calculated with time-dependent DFT (TD-DFT). The total energies of all those states of the molecules in different dielectric environments were separately obtained from DFT single-point energy calculations.

With the help of Figure 12b, the calculated energies of the respective states can be used to extract the ionization energy as $\text{IE}(S_0) = E(\text{cation}) - E(S_0)$, the electron affinity as $-\text{EA}(S_0) = E(\text{anion}) - E(S_0)$, and the optical gap as $E_{\text{opt}} = E(S_1) - E(S_0)$. Since $E(S_0)$ is contained in all these equations, it is convenient to use this as the reference energy $E = 0$ in the states picture. We emphasize that those energies represent vertical transitions between the respective states as the coordinates of the nuclei remained constant for the computations.

Because the transition energies $\text{IE}(S_0)$, $\text{EA}(S_0)$, and E_{opt} should be invariant for a given system, one can now transfer the above information into an energy level diagram, as depicted in Figure 12a, by using $\text{IE}(S_0) = E_{\text{vac}} - H_0^{+1}$ as well as $\text{EA}(S_0) = E_{\text{vac}} - L_0^{-1}$ and by conveniently setting E_{vac} as the reference energy $E = 0$ in the energy levels picture. It follows that the transport gap is $E_{\text{trans}} = L_0^{-1} - H_0^{+1} = \text{IE}(S_0) - \text{EA}(S_0)$. The exciton binding energy is obtained as $E_{\text{B}} = E_{\text{trans}} - E_{\text{opt}}$ and amounts to $E_{\text{B}} = E_{\text{C}}^+ + E_{\text{C}}^- + E_{\text{rel}}^{\text{exc}}$ according to our model.^[17] Further details are found in our previous work.^[24] The computational results are summarized in Table 3 along with the main experimental results depicted in Figure 12 and additional theoretical studies.

Quite interestingly, the statements $E_{\text{C}}^+ \approx E_{\text{C}}^-$ and $P^+ \approx P^-$ are excellently fulfilled for pentacene in the environments considered here, which corroborates our initial assumption. If deviations occur between P^+ and P^- , they turn out to be smaller than 0.1 eV in the above theoretical studies,^[24,118,126] so that we refrain here from assigning different values for P^+ and P^- in the evaluation of the experimental data. In all cases, the polarization energies (positive as well as negative) calculated for pentacene adsorbed on graphite are similar to the values extracted from the experiments, and this accordance attests to the consistency

of the interpretation of the complementary spectroscopic techniques.

Moreover, all calculations yielded transport gaps (and an optical gap in the case of TD-DFT) somewhat smaller than the respective measured gaps. Yet, the difference between both gaps, $E_{\text{B}} = E_{\text{trans}} - E_{\text{opt}}$, in our calculations for gas-phase pentacene^[24] agrees almost perfectly with the experimental value, presumably due to a cancellation of computational errors. From $E_{\text{B}}(\text{calculated}) \approx E_{\text{B}}(\text{measured})$ and from $E_{\text{B}} = E_{\text{C}}^+ + E_{\text{C}}^- + E_{\text{rel}}^{\text{exc}}$ it follows that the computed excited state relaxation energy $E_{\text{rel}}^{\text{exc}} = 0.29$ eV can be judged as reliable, and this value is indeed used in Figure 12.

Furthermore, if $E_{\text{rel}}^{\text{exc}} = 0.29$ eV is approximately also valid for the flat-lying pentacene ML on graphite, then one obtains the position $L_0 = -3.04$ eV (via extrapolation from $L_0^{\text{g}} = -3.33$ eV), while all other quantities are already depicted in Figure 12. Consequently, the HOMO and LUMO levels unaffected by perturbations from the spectroscopic probe processes for pentacene in the gas-phase ($H_0 = -5.32$ eV and $L_0 = -2.72$ eV) and adsorbed flat-lying on graphite ($H_0 = -5.46$ eV and $L_0 = -3.04$ eV) were consistently determined with respect to the vacuum level at $E_{\text{vac}} = 0$ eV.

4. Conclusion

In this perspective we briefly surveyed several important state-of-the-art spectroscopic techniques whose surface sensitivities and spectral resolutions are adequate to investigate molecular films in the ML regime up to thicknesses of tens of nanometers. The characterization of the electronic and optical properties of organic samples (single molecules and condensed adsorbate layers) is important for fundamental research, and it also yields valuable data for potential (opto-)electronic applications. The problem, however, is that these spectroscopies involve non-negligible perturbations of the investigated molecules. We demonstrated that the proper consideration of the initial and final states of the probe processes is essential for a quantitatively accurate interpretation of the primary data. To this end, a previously

introduced model applicable to molecules in weakly interacting environments was adapted.^[17] This model was first applied to tetraphenylidibenzoperiflanthene (CAS registry number: 175606-05-0) on graphite,^[24] where all key quantities (except for the EA in the gas phase) were acquired by means of UPS, 2PPE, LEIPS, and DRS, supplemented by theoretical considerations.

We identified on-site Coulomb energies (the so-called “charging energies”) as the main reason for the discrepancy of the measured spectroscopic data from the unperturbed energy levels of a given molecule. On the basis of the charging energies and the polarization energies of charged states in a polarizable environment these differences can be reconciled, and quantitatively accurate energy diagrams can be obtained. We have shown this for pentacene single molecules and face-on adsorbed MLs on graphite, where the wealth of spectroscopic data from the literature can be understood in a consistent manner. From the remarkable agreement between experimental and theoretical results we conclude that the assumptions of the model (among other things: all spectroscopic transitions are vertical, no hybridization occurs, and the individual molecules are regarded as chargeable entities) are very reasonably fulfilled here. Those energy diagrams can therefore be considered as a benchmark example, and applying the same model to other weakly interacting molecular systems should yield valuable reference data.

Quite importantly, the measured spectra depend sensitively on the microscopic structures of the adsorbed molecular films owing to a variety of aggregation effects (e.g., distinct electronic band formation, different dielectric properties depending on the film thickness, and coupling of optical transition dipole moments). For pentacene, in particular, the typically observed face-on and short-edge-on molecular orientations with respect to a substrate surface result in sizable distinctions in the recorded spectra. Our evaluation presented here is valid for face-on oriented pentacene on weakly interacting substrates such as graphite. Precise structural information on the molecular level is therefore a prerequisite for the analysis of energy levels. This is especially important for organic compounds that are prone to polymorphism.

Finally, we emphasize that the available spectroscopic database for pentacene, chosen here as a prime example, is one of the most comprehensive among the organic molecular substances. While this fact as such is certainly beneficial, it also requires a systematization of the various datasets, in order to avoid confusion of spectroscopic data and corresponding theoretical calculations for disparate microscopic film structures, for example. For many other molecular systems, it is more the rule than the exception that the current database is insufficient. As a prominent example we discussed the intensively studied system CuPc/PTCDA/Ag(111) for which no experimental data for the CuPc LUMO are available to the best of our knowledge.

On a broader scale, we hope that this perspective stimulates discussions between the scientific communities concerned with spectroscopic techniques, structural characterization methods, theoretical calculations and simulations, as well as device-related developments, because we firmly believe that they all share a common interest in deciphering the structure–property relations of organic materials.^[127,128]

Acknowledgements

This work was financed in part by the Deutsche Forschungsgemeinschaft (DFG) project “Hybridization of Organic Molecules with Metal Substrates in the Presence of Surface Passivation Layers” (FR 875/16-1). T.K. thanks the Evonik Stiftung for providing a Ph.D. scholarship. Open access funding enabled and organized by Projekt DEAL.

Conflict of Interest

The authors declare no conflict of interest.

Keywords

charging energies, electronic and optical properties, energy level diagrams, molecular states, polarizable continuum models, spectroscopic techniques, surface sensitivity

Received: January 29, 2021

Revised: March 26, 2021

Published online: May 10, 2021

- [1] S. Reineke, *Nat. Mater.* **2015**, *14*, 459.
- [2] G. J. Hedley, A. Ruseckas, I. D. W. Samuel, *Chem. Rev.* **2017**, *117*, 796.
- [3] S. Olthof, S. Mehraeen, S. K. Mohapatra, S. Barlow, V. Coropceanu, J.-L. Brédas, S. R. Marder, A. Kahn, *Phys. Rev. Lett.* **2012**, *109*, 176601.
- [4] M. L. Tietze, P. Pahnner, K. Schmidt, K. Leo, B. Lüssem, *Adv. Funct. Mater.* **2015**, *25*, 2701.
- [5] A. J. Cruz-Cabeza, S. M. Reutzel-Edens, J. Bernstein, *Chem. Soc. Rev.* **2015**, *44*, 8619.
- [6] A. J. Cruz-Cabeza, N. Feeder, R. J. Davey, *Commun. Chem.* **2020**, *3*, 142.
- [7] J. Simbrunner, B. Schrode, S. Hofer, J. Domke, T. Fritz, R. Forker, R. Resel, *J. Phys. Chem. C* **2021**, *125*, 618.
- [8] V. Coropceanu, J. Cornil, D. A. da Silva Filho, Y. Olivier, R. Silbey, J.-L. Brédas, *Chem. Rev.* **2007**, *107*, 926.
- [9] K. Walzer, B. Maennig, M. Pfeiffer, K. Leo, *Chem. Rev.* **2007**, *107*, 1233.
- [10] I. Salzmann, G. Heimel, M. Oehzelt, S. Winkler, N. Koch, *Acc. Chem. Res.* **2016**, *49*, 370.
- [11] C. Gaul, S. Hutsch, M. Schwarze, K. S. Schellhammer, F. Bussolotti, S. Kera, G. Cuniberti, K. Leo, F. Ortman, *Nat. Mater.* **2018**, *17*, 439.
- [12] M. Schwarze, C. Gaul, R. Scholz, F. Bussolotti, A. Hofacker, K. S. Schellhammer, B. Nell, B. D. Naab, Z. Bao, D. Spoltore, K. Vandewal, J. Widmer, S. Kera, N. Ueno, F. Ortman, K. Leo, *Nat. Mater.* **2019**, *18*, 242.
- [13] C. Zwick, A. Baby, M. Gruenewald, E. Verwüster, O. T. Hofmann, R. Forker, G. Fratesi, G. P. Brivio, E. Zojer, T. Fritz, *ACS Nano* **2016**, *10*, 2365.
- [14] C. Zwick, M. Meissner, F. Sojka, R. Forker, T. Fritz, *Phys. Rev. Mater.* **2019**, *3*, 085604.
- [15] F. Otto, T. Kirchhübel, A. Baby, F. Sojka, G. Fratesi, T. Fritz, R. Forker, *J. Phys. Chem. C* **2020**, *124*, 4114.
- [16] X.-Y. Zhu, *J. Phys. Chem. Lett.* **2014**, *5*, 2283.
- [17] T. Kirchhübel, O. L. A. Monti, T. Munakata, S. Kera, R. Forker, T. Fritz, *Phys. Chem. Chem. Phys.* **2019**, *21*, 12730.
- [18] M. Knupfer, *Appl. Phys. A* **2003**, *77*, 623.

- [19] L. Zhu, Y. Yi, Z. Wei, *J. Phys. Chem. C* **2018**, *122*, 22309.
- [20] A. Baby, M. Gruenewald, C. Zwick, F. Otto, R. Forker, G. van Straaten, M. Franke, B. Stadtmüller, C. Kumpf, G. P. Brivio, G. Fratesi, T. Fritz, E. Zojer, *ACS Nano* **2017**, *11*, 10495.
- [21] S. Olthof, R. Meerheim, M. Schober, K. Leo, *Phys. Rev. B* **2009**, *79*, 245308.
- [22] M. Schober, M. Anderson, M. Thomschke, J. Widmer, M. Furno, R. Scholz, B. Lüssem, K. Leo, *Phys. Rev. B* **2011**, *84*, 165326.
- [23] M. Mesta, M. Carvelli, R. J. de Vries, H. van Eersel, J. J. M. van der Holst, M. Schober, M. Furno, B. Lüssem, K. Leo, P. Loebel, R. Coehoorn, P. A. Bobbert, *Nat. Mater.* **2013**, *12*, 652.
- [24] T. Kirchhübel, S. Kera, T. Munakata, N. Ueno, R. Shiraiishi, T. Yamaguchi, K. Yonezawa, T. Ueba, F. Bussolotti, J. Yang, T. Yamada, R. Mori, S. Kunieda, T. Huempfer, M. Gruenewald, R. Forker, T. Fritz, *J. Phys. Chem. C* **2020**, *124*, 19622.
- [25] O. L. Griffith, J. E. Anthony, A. G. Jones, D. L. Lichtenberger, *J. Am. Chem. Soc.* **2010**, *132*, 580.
- [26] S. Maruyama, Y. Takeyama, Y. Matsumoto, *Appl. Phys. Express* **2011**, *4*, 051602.
- [27] A. Damascelli, Z. Hussain, Z.-X. Shen, *Rev. Mod. Phys.* **2003**, *75*, 473.
- [28] F. Reinert, S. Hüfner, *New J. Phys.* **2005**, *7*, 97.
- [29] N. Ueno, S. Kera, *Prog. Surf. Sci.* **2008**, *83*, 490.
- [30] S. Kera, N. Ueno, *J. Electron Spectrosc. Relat. Phenom.* **2015**, *204*, 2.
- [31] Y. Nakayama, S. Kera, N. Ueno, *J. Mater. Chem. C* **2020**, *8*, 9090.
- [32] V. Coropceanu, M. Malagoli, D. A. da Silva Filho, N. E. Gruhn, T. G. Bill, J. L. Brédas, *Phys. Rev. Lett.* **2002**, *89*, 275503.
- [33] H. Yamane, S. Nagamatsu, H. Fukagawa, S. Kera, R. Friedlein, K. K. Okudaira, N. Ueno, *Phys. Rev. B* **2005**, *72*, 153412.
- [34] H. Fukagawa, H. Yamane, T. Kataoka, S. Kera, M. Nakamura, K. Kudo, N. Ueno, *Phys. Rev. B* **2006**, *73*, 245310.
- [35] N. Koch, A. Vollmer, I. Salzmann, B. Nickel, H. Weiss, J. P. Rabe, *Phys. Rev. Lett.* **2006**, *96*, 156803.
- [36] H. Yoshida, *Chem. Phys. Lett.* **2012**, *539–540*, 180.
- [37] H. Yoshida, *Rev. Sci. Instrum.* **2013**, *84*, 103901.
- [38] H. Yoshida, *Rev. Sci. Instrum.* **2014**, *85*, 016101.
- [39] H. Yoshida, *J. Electron Spectrosc. Relat. Phenom.* **2015**, *204*, 116.
- [40] H. Yoshida, K. Yamada, J. Tsutsumi, N. Sato, *Phys. Rev. B* **2015**, *92*, 075145.
- [41] F. Schedin, G. Thornton, *Rev. Sci. Instrum.* **1997**, *68*, 41.
- [42] I. G. Hill, A. Kahn, Z. G. Soos, R. A. Pascal Jr., *Chem. Phys. Lett.* **2000**, *327*, 181.
- [43] W. Han, H. Yoshida, N. Ueno, S. Kera, *Appl. Phys. Lett.* **2013**, *103*, 123303.
- [44] Y. Kashimoto, K. Yonezawa, M. Meissner, M. Gruenewald, T. Ueba, S. Kera, R. Forker, T. Fritz, H. Yoshida, *J. Phys. Chem. C* **2018**, *122*, 12090.
- [45] K. Yamada, S. Yanagisawa, T. Koganezawa, K. Mase, N. Sato, H. Yoshida, *Phys. Rev. B* **2018**, *97*, 245206.
- [46] A. Sugie, W. Han, N. Shioya, T. Hasegawa, H. Yoshida, *J. Phys. Chem. C* **2020**, *124*, 9765.
- [47] M. Terashima, T. Miyayama, T. Shirao, H. W. Mo, Y. Hatae, H. Fujimoto, K. Watanabe, *Surf. Interface Anal.* **2020**, *52*, 948.
- [48] Y. Uemura, S. A. Abd-Rahman, S. Yanagisawa, H. Yoshida, *Phys. Rev. B* **2020**, *102*, 125302.
- [49] J. B. Pendry, *Phys. Rev. Lett.* **1980**, *45*, 1356.
- [50] J. B. Pendry, *J. Phys. C: Solid State Phys.* **1981**, *14*, 1381.
- [51] H. Proehl, R. Nitsche, T. Dienel, K. Leo, T. Fritz, *Phys. Rev. B* **2005**, *71*, 165207.
- [52] R. Forker, T. Fritz, *Phys. Chem. Chem. Phys.* **2009**, *11*, 2142.
- [53] R. Forker, M. Gruenewald, T. Fritz, *Annu. Rep. Prog. Chem., Sect. C: Phys. Chem.* **2012**, *108*, 34.
- [54] S. B. Jo, H. H. Kim, H. Lee, B. Kang, S. Lee, M. Sim, M. Kim, W. H. Lee, K. Cho, *ACS Nano* **2015**, *9*, 8206.
- [55] C. Schünemann, D. Wynands, K.-J. Eichhorn, M. Stamm, K. Leo, M. Riede, *J. Phys. Chem. C* **2013**, *117*, 11600.
- [56] D. E. Aspnes, A. A. Studna, *Phys. Rev. Lett.* **1985**, *54*, 1956.
- [57] R. J. Cole, B. G. Frederick, P. Weightman, *J. Vac. Sci. Technol., A* **1998**, *16*, 3088.
- [58] P. Weightman, D. S. Martin, A. Maunder, *J. Electron Spectrosc. Relat. Phenom.* **2001**, *114–116*, 1069.
- [59] H. Zaglmayr, C. G. Hu, L. D. Sun, P. Zeppenfeld, *Meas. Sci. Technol.* **2014**, *25*, 115603.
- [60] L. Zhang, X. Fu, M. Hohage, P. Zeppenfeld, L. D. Sun, *Phys. Rev. Mater.* **2017**, *1*, 043401.
- [61] M. Gruenewald, K. Wachter, M. Meissner, M. Kozlik, R. Forker, T. Fritz, *Org. Electron.* **2013**, *14*, 2177.
- [62] K. Broch, U. Heinemeyer, A. Hinderhofer, F. Anger, R. Scholz, A. Gerlach, F. Schreiber, *Phys. Rev. B* **2011**, *83*, 245307.
- [63] P. Sony, A. Shukla, *Phys. Rev. B* **2007**, *75*, 155208.
- [64] A. Hinderhofer, U. Heinemeyer, A. Gerlach, S. Kowarik, R. M. J. Jacobs, Y. Sakamoto, T. Suzuki, F. Schreiber, *J. Chem. Phys.* **2007**, *127*, 194705.
- [65] N. Shioya, R. Murdey, K. Nakao, H. Yoshida, T. Koganezawa, K. Eda, T. Shimoaka, T. Hasegawa, *Sci. Rep.* **2019**, *9*, 579.
- [66] T. Aoki-Matsumoto, K. Furuta, T. Yamada, H. Moriya, K. Mizuno, A. H. Matsui, *Int. J. Mod. Phys. B* **2001**, *15*, 3753.
- [67] R. He, X. Chi, A. Pinczuk, D. V. Lang, A. P. Ramirez, *Appl. Phys. Lett.* **2005**, *87*, 211117.
- [68] S. P. Park, S. S. Kim, J. H. Kim, C. N. Whang, S. Im, *Appl. Phys. Lett.* **2002**, *80*, 2872.
- [69] R. He, N. G. Tassi, G. B. Blanchet, A. Pinczuk, *Appl. Phys. Lett.* **2010**, *96*, 263303.
- [70] R. He, N. G. Tassi, G. B. Blanchet, A. Pinczuk, *Appl. Phys. Lett.* **2005**, *87*, 103107.
- [71] Y. P. Piryatinski, M. V. Kurik, *Ukr. J. Phys.* **2011**, *56*, 1048.
- [72] F. Anger, J. O. Ossó, U. Heinemeyer, K. Broch, R. Scholz, A. Gerlach, F. Schreiber, *J. Chem. Phys.* **2012**, *136*, 054701.
- [73] H. Y. Mao, F. Bussolotti, D.-C. Qi, R. Wang, S. Kera, N. Ueno, A. T. S. Wee, W. Chen, *Org. Electron.* **2011**, *12*, 534.
- [74] K. Kuhnke, R. Becker, M. Epple, K. Kern, *Phys. Rev. Lett.* **1997**, *79*, 3246.
- [75] W. Gebauer, A. Langner, M. Schneider, M. Sokolowski, E. Umbach, *Phys. Rev. B* **2004**, *69*, 155431.
- [76] J. D. E. McIntyre, D. E. Aspnes, *Surf. Sci.* **1971**, *24*, 417.
- [77] R. Forker, C. Golnik, G. Pizzi, T. Dienel, T. Fritz, *Org. Electron.* **2009**, *10*, 1448.
- [78] T. Dienel, C. Loppacher, S. C. B. Mannsfeld, R. Forker, T. Fritz, *Adv. Mater.* **2008**, *20*, 959.
- [79] M. Hoffmann, K. Schmidt, T. Fritz, T. Hasche, V. M. Agranovich, K. Leo, *Chem. Phys.* **2000**, *258*, 73.
- [80] R. Forker, T. Dienel, A. Krause, M. Gruenewald, M. Meissner, T. Kirchhübel, O. Gröning, T. Fritz, *Phys. Rev. B* **2016**, *93*, 165426.
- [81] M. Meissner, M. Gruenewald, F. Sojka, C. Udhardt, R. Forker, T. Fritz, *Surf. Sci.* **2012**, *606*, 1709.
- [82] F. S. Tautz, M. Eremitchenko, J. A. Schaefer, M. Sokolowski, V. Shklover, E. Umbach, *Phys. Rev. B* **2002**, *65*, 125405.
- [83] Y. Zou, L. Kilian, A. Schöll, T. Schmidt, R. Fink, E. Umbach, *Surf. Sci.* **2006**, *600*, 1240.
- [84] M. Häming, M. Greif, M. Wießner, A. Schöll, F. Reinert, *Surf. Sci.* **2010**, *604*, 1619.
- [85] M. Häming, M. Greif, C. Sauer, A. Schöll, F. Reinert, *Phys. Rev. B* **2010**, *82*, 235432.
- [86] J. Ziroff, F. Forster, A. Schöll, P. Puschnig, F. Reinert, *Phys. Rev. Lett.* **2010**, *104*, 233004.
- [87] T. Dienel, A. Krause, R. Alle, R. Forker, K. Meerholz, T. Fritz, *Adv. Mater.* **2010**, *22*, 4064.

- [88] M. Gruenewald, L. K. Schirra, P. Winget, M. Kozlik, P. F. Ndione, A. K. Sigdel, J. J. Berry, R. Forker, J.-L. Brédas, T. Fritz, O. L. A. Monti, *J. Phys. Chem. C* **2015**, *119*, 4865.
- [89] A. Lerch, J. E. Zimmermann, A. Namgalies, K. Stallberg, U. Höfer, *J. Phys.: Condens. Matter* **2018**, *30*, 494001.
- [90] H. Petek, S. Ogawa, *Prog. Surf. Sci.* **1997**, *56*, 239.
- [91] P. M. Echenique, R. Berndt, E. V. Chulkov, T. Fauster, A. Goldmann, U. Höfer, *Surf. Sci. Rep.* **2004**, *52*, 219.
- [92] X.-Y. Zhu, *Surf. Sci. Rep.* **2004**, *56*, 1.
- [93] T. Yamada, T. Munakata, *Prog. Surf. Sci.* **2018**, *93*, 108.
- [94] K. Glöckler, C. Seidel, A. Soukopp, M. Sokolowski, E. Umbach, M. Böhringer, R. Berndt, W.-D. Schneider, *Surf. Sci.* **1998**, *405*, 1.
- [95] L. Kilian, E. Umbach, M. Sokolowski, *Surf. Sci.* **2004**, *573*, 359.
- [96] B. Stadtmüller, T. Sueyoshi, G. Kichin, I. Kröger, S. Soubatch, R. Temirov, F. S. Tautz, C. Kumpf, *Phys. Rev. Lett.* **2012**, *108*, 106103.
- [97] M. Gruenewald, C. Sauer, J. Peuker, M. Meissner, F. Sojka, A. Schöll, F. Reinert, R. Forker, T. Fritz, *Phys. Rev. B* **2015**, *91*, 155432.
- [98] S. Krause, M. B. Casu, A. Schöll, E. Umbach, *New J. Phys.* **2008**, *10*, 085001.
- [99] T. Graber, F. Forster, A. Schöll, F. Reinert, *Surf. Sci.* **2011**, *605*, 878.
- [100] I. Kröger, B. Stadtmüller, C. Stadler, J. Zirotto, M. Kochler, A. Stahl, F. Pollinger, T.-L. Lee, J. Zegenhagen, F. Reinert, *New J. Phys.* **2010**, *12*, 083038.
- [101] I. Kröger, B. Stadtmüller, C. Kumpf, *New J. Phys.* **2016**, *18*, 113022.
- [102] H. Peisert, T. Schwiager, J. M. Auerhammer, M. Knupfer, M. S. Golden, J. Fink, *J. Appl. Phys.* **2001**, *90*, 466.
- [103] S. W. Cho, L. F. J. Piper, A. DeMasi, A. R. H. Preston, K. E. Smith, K. V. Chauhan, P. Sullivan, R. A. Hatton, T. S. Jones, *J. Phys. Chem. C* **2010**, *114*, 1928.
- [104] D. Lüftner, M. Milko, S. Huppmann, M. Scholz, N. Ngyuen, M. Wiefßner, A. Schöll, F. Reinert, P. Puschnig, *J. Electron Spectrosc. Relat. Phenom.* **2014**, *195*, 293.
- [105] N. Marom, O. Hod, G. E. Scuseria, L. Kronik, *J. Chem. Phys.* **2008**, *128*, 164107.
- [106] D. A. Egger, V. G. Ruiz, W. A. Saidi, T. Bučko, A. Tkatchenko, E. Zojer, *J. Phys. Chem. C* **2013**, *117*, 3055.
- [107] B. Stadtmüller, M. Willenbockel, S. Schröder, C. Kleimann, E. M. Reinisch, T. Ules, S. Soubatch, M. G. Ramsey, F. S. Tautz, C. Kumpf, *Phys. Rev. B* **2015**, *91*, 155433.
- [108] S. Thussing, P. Jakob, *J. Phys. Chem. C* **2017**, *121*, 13680.
- [109] G. Dutton, X.-Y. Zhu, *J. Phys. Chem. B* **2002**, *106*, 5975.
- [110] E. Abad, C. González, J. Ortega, F. Flores, *Org. Electron.* **2010**, *11*, 332.
- [111] I. Fernández Torrente, K. J. Franke, J. I. Pascual, *J. Phys.: Condens. Matter* **2008**, *20*, 184001.
- [112] T. Masubuchi, Y. Sugawara, A. Nakajima, *J. Chem. Phys.* **2016**, *145*, 244306.
- [113] E. V. Tsiper, Z. G. Soos, W. Gao, A. Kahn, *Chem. Phys. Lett.* **2002**, *360*, 47.
- [114] D. Cahen, A. Kahn, E. Umbach, *Mater. Today* **2005**, *8*, 32.
- [115] S. Duhm, G. Heimel, I. Salzmann, H. Glowatzki, R. L. Johnson, A. Vollmer, J. P. Rabe, N. Koch, *Nat. Mater.* **2008**, *7*, 326.
- [116] J. Sauther, J. Wüsten, S. Lach, C. Ziegler, *J. Chem. Phys.* **2009**, *131*, 034711.
- [117] T. M. Halasinski, D. M. Hudgins, F. Salama, L. J. Allamandola, T. Bally, *J. Phys. Chem. A* **2000**, *104*, 7484.
- [118] J. B. Neaton, M. S. Hybertsen, S. G. Louie, *Phys. Rev. Lett.* **2006**, *97*, 216405.
- [119] S. L. Murov, I. Carmichael, G. L. Hug, *Handbook of Photochemistry*, Dekker, New York **1993**.
- [120] R. Dabestani, I. N. Ivanov, *Photochem. Photobiol.* **1999**, *70*, 10.
- [121] J. Li, I. Duchemin, O. M. Roscioni, P. Friederich, M. Anderson, E. Da Como, G. Kociok-Köhn, W. Wenzel, C. Zannoni, D. Beljonne, X. Blase, G. D'Avino, *Mater. Horiz.* **2019**, *6*, 107.
- [122] L. Crocker, T. Wang, P. Kebarle, *J. Am. Chem. Soc.* **1993**, *115*, 7818.
- [123] G. Rouillé, T. Kirchhübel, M. Rink, M. Gruenewald, J. Kröger, R. Forker, T. Fritz, *Phys. Chem. Chem. Phys.* **2015**, *17*, 30404.
- [124] A. A. Radzig, B. M. Smirnov, in *Reference Data on Atoms, Molecules, and Ions* (Ed: J. P. Toennies), Springer, Heidelberg, Germany **1985**.
- [125] J. Tomasi, B. Mennucci, R. Cammi, *Chem. Rev.* **2005**, *105*, 2999.
- [126] S. Yanagisawa, *Jpn. J. Appl. Phys.* **2020**, *59*, 031002.
- [127] C. Poelking, M. Tietze, C. Elschner, S. Olthof, D. Hertel, B. Baumeier, F. Würthner, K. Meerholz, K. Leo, D. Andrienko, *Nat. Mater.* **2015**, *14*, 434.
- [128] G. D'Avino, L. Muccioli, F. Castet, C. Poelking, D. Andrienko, Z. G. Soos, J. Cornil, D. Beljonne, *J. Phys.: Condens. Matter* **2016**, *28*, 433002.



Roman Forker studied physics at the University of Technology Dresden, Germany, and received his doctoral degree (Dr. rer. nat.) in 2010 for his experimental studies on epitaxial organic layers, supervised by Prof. Karl Leo. Since 2010 he has been working as a staff scientist in the group of Prof. Torsten Fritz at the Friedrich Schiller University Jena, Germany. Research stays at the University of Arizona, Tucson, United States (Prof. Neal R. Armstrong) and at Osaka University, Japan (Prof. Toshiaki Munakata) further shaped his research interests, which revolve around the structure–property relationships of organic materials.



Marco Gruenewald studied physics at the Friedrich Schiller University Jena, Germany. He received his doctoral degree (Dr. rer. nat.) in Jena in 2017 for experimental work on ultrathin organic layers, supervised by Prof. Torsten Fritz. Since 2017 he has been employed as a staff scientist in the group of Prof. Torsten Fritz. His research interests include the investigation of the structure–property relationships of organic thin films, especially using optical and photoelectron spectroscopies.



Tino Kirchhübel studied physics at the Friedrich Schiller University Jena, Germany, where he obtained his master's degree in 2014. The same year, he worked as a visiting researcher in the group of Prof. Toshiaki Munakata at Osaka University, Japan, and continued his studies in the group of Prof. Torsten Fritz at the Friedrich Schiller University Jena, Germany. His research work comprises the structure–property relationships of thin films based on small organic molecules examined with experimental and computational techniques, and recently he focused on the coherent interpretation of spectroscopic data in the field of molecular science.



Torsten Fritz studied physics and mathematics at the University of Technology Dresden, Germany. In 1989, he obtained his doctoral degree from the same university for experimental work on evaporated dye layers. In the following years he became increasingly interested in highly ordered organic thin films prepared by organic molecular beam epitaxy. He was appointed in 2009 as full professor of solid state physics at the Friedrich Schiller University Jena, Germany. His current research interests encompass structure–property relations in organic ultrathin films, studied by various surface science methods including scanning tunneling microscopy, low-energy electron diffraction, surface-sensitive optical spectroscopy, and photoelectron spectroscopies.